International Journal of Humanoid Robotics
(2021) 2150015 (35 pages)

DOI: 10.1142/S0219843621500158

World Scientific
www.worldscientific.com

A Nonlinear Optimal Control Approach for Multi-DOF Brachiation Robots

G. Rigatos*

Unit of Industrial Automation
Industrial Systems Institute
Rion Patras 26504, Greece
grigat@ieee.org

M. Abbaszadeh

GE Global Research, General Electric
Niskayuna 12309, NY, USA
masouda@ualberta.ca

K. Busawon

Department of Mechanical Engineering
University of Northumbria
Newcastle NE1 8ST, UK
krishna.busawon@northumbria.ac.uk

Z. Gao

Department of Electrical Engineering
University of Northumbria
Newcastle NE1 8ST, UK
zhiwei.gao@northumbria.ac.uk

J. Pomares

Department of Physics, Systems Engineering and Signal Theory
University of Alicante
Alicante 03690, Spain
jpomares@gcloud.ua.es

Received 24 June 2020
Revised 23 December 2020
Accepted 17 September 2021
Published

This paper proposes a nonlinear optimal control approach for mulitple degrees of freedom (DOF) brachiation robots, which are often used in inspection and maintenance tasks of the electric power grid. Because of the nonlinear and multivariable structure of the related state-

*Corresponding author.

space model, as well as because of underactuation, the control problem of these robots is nontrivial. The dynamic model of the brachiation robots undergoes first approximate linearization with the use of Taylor series expansion around a temporary operating point which is recomputed at each iteration of the control method. For the approximately linearized model, an H-infinity feedback controller is designed. The linearization procedure relies on the Jacobian matrices of the brachiation robots' state-space model. The proposed control method stands for the solution of the optimal control problem for the nonlinear and multivariable dynamics of the brachiation robots, under model uncertainties and external perturbations. For the computation of the controller's feedback gains an algebraic Riccati equation is solved at each time-step of the control method. The global stability properties of the control scheme are proven through Lyapunov analysis. The new nonlinear optimal control approach achieves fast and accurate tracking for all state variables of the brachiation robots, under moderate variations of the control inputs.

Keywords: Brachiation robots; underactuated robots; nonlinear dynamics; nonlinear H-infinity control; nonlinear optimal control; robust control; global stability.

1. Introduction

The control problem of brachiation robots is important because these robots can be used in inspection and maintenance tasks for critical infrastructures, such as bridges, dams, buildings or the electric power transmission and distribution system.[1–3] This control problem exhibits significant difficulty because of the nonlinear and multivariable structure of the brachiation robots' state-space model.[4–6] The control problem becomes even more complicated when one considers that brachiation robots are often underactuated.[7–9] On the one side, underactuation may be pursued in the design of these robotic systems in an aim to reduce their weight and energy consumption after removing specific actuators from them. On the other side, functioning of these robotic systems in an underactuation mode signifies that these robots are fault tolerant in the case of actuators' failures and that they continue to perform reliably their tasks even if specific actuators are subjected to a fault.[10–12] So far, several nonlinear control methods have been proposed for these robotic systems.[13–15] There have been several attempts to treat the related control problem with the use of global linearization-based techniques or with the use of robust control methods such as sliding-mode control. There have been also several results on the use of model predictive control (MPC) on these robotic systems.[16–19] The confirmation of the global stability and of convergence to an optimum for such control methods remains a challenge.[20–22] This research area remains open for further advancements and additional results on the control of brachiate and bi-brachiate robots can be found in Refs. 23–29.

In this paper, a novel nonlinear optimal (H-infinity) control method is developed for multi-DOF underactuated brachiation robots. To this end, the dynamic model of the brachiation robots undergoes first approximate linearization around a temporary operating point which is updated at each time-step of the control method.[30–34] This linearization point is defined by the present value of the state vector and by the last sampled value of the control inputs vector. The linearization process is based on first-order Taylor series expansion and on the computation of the related Jacobian matrices.[35–37] The modeling error which is due to the truncation of higher-order terms from the Taylor series is considered to be a perturbation, that is, asymptotically compensated by the robustness of the control scheme. For the approximately linearized model of the brachiation robots, a stabilizing *H*-infinity feedback controller is designed. The proposed *H*-infinity control achieves the solution of the optimal control problem for the nonlinear dynamics of the brachiation robots, under model uncertainty and external perturbations.

Actually, this controller represents a min–max differential game in which the control inputs try to minimize a cost function that comprises a quadratic term of the state vector's tracking error, while the model uncertainty and exogenous disturbance terms try to maximize this cost function. To compute the feedback gains of the *H*-infinity controller an algebraic Riccati equation is repetitively solved at each iteration of the control algorithm.[38,39] The stability properties of the control method are proven through Lyapunov analysis. First, it is proven that the control system satisfies the *H*-infinity tracking performance criterion, which signifies elevated robustness against modeling errors and disturbances.[8,40] Moreover, under moderate conditions, it is proven that the control system of the brachiation robots is globally asymptotically stable.[8] To implement state estimation-based control without the need to measure the entire state vector of the brachiation robot, the *H*-infinity Kalman filter is used as a robust state estimator.[8]

This paper's nonlinear optimal control method is a novel and significant result. Preceding approaches about the use of *H*-infinity control in nonlinear dynamical systems were limited to the case of affine-in-the-input systems with drift-only dynamics and considered that the control inputs gain matrix is not dependent of the values of the system's state vector. Moreover, in these approaches, linearization was performed around points of the desirable trajectory whereas in this paper's control method the linearization points are related with the value of the state vector at each sampling instant as well as with the last sampled value of the control inputs vector. The Riccati equation which has been proposed for computing the feedback gains of the controller is novel, so is the presented global stability proof through Lyapunov analysis.

The structure of this paper is as follows: In Sec. 2, the dynamic model of the multi-DOF brachiation robot is analyzed with the use of the Euler–Lagrange method and the related state-space description is obtained. In Sec. 3, approximate linearization is performed for the state-space model of the brachiation robot using Taylor series expansion and the computation of the related Jacobian matrices. Next, a stabilizing *H*-infinity feedback controller is designed for this robotic system. In Sec. 4, the global stability properties of the control method are proven through Lyapunov analysis. Moreover, to perform state estimation-based control the *H*-infinity Kalman filter is used as a robust state estimator. In Sec. 5, the fine performance of the control method is further confirmed through simulation experiments. Finally, in Sec. 6, concluding remarks are stated.

2. Dynamic Model of the Multi-DOF Brachiation Robot

The diagram of a brachiation robot which is used for inspection and maintenance of cables of the power grid is shown in Fig. 1. The dynamic model of brachiation robot is

$$M(\theta)\,\ddot{\theta} + C(\theta,\dot{\theta}) + G(\theta) = B\tau - F_v(\dot{\theta}), \tag{1}$$

where $\theta = [\theta_1, \theta_2, \theta_3]^T$ is the vector of the joints' angles, $M(\theta)$ is the inertia matrix, $C(\theta,\dot{\theta})$ is the Coriolis and centrifugal terms vector, $G(\theta)$ is the gravitational terms vector, $\bar{B}\tau$ is the control input torques vector with matrix $\bar{B}$ to denote the specific type of underactuation, and $F_v(\dot{\theta})$ is a vector of viscous torques.

The lengths of the three links are denoted as l_i $i = 1, 2, 3$, while it is considered that l_1 and l_2 are greater than or equal to l_3. It is assumed that the masses of the three links are concentrated on the links' center of gravity. I_1, I_2 and I_3 are the moments of inertia of the three links of the considered brachiation robot, while b_1, b_2 and b_3 are friction coefficients defining the friction torques that appear in the joints of the above-noted links.

Using Euler–Lagrange analysis, one obtains the dynamic model of the brachiation robot which comprises the following three differential equations: (the detailed proof has been given in Appendix A)

$$\begin{aligned}&\left[m_1\frac{l_1^2}{2} + I_1 + m_2 l_1^2 + m_2\frac{l_2^2}{4} + I_2 + m_3 l_1^2 + m_3\frac{l_3^2}{4} + m_2 l_1 l_2\cos(\theta_2) + I_3\right.\\ &\quad\left. + m_3 l_1 l_3\cos(\theta_3)\right]\ddot{\theta}_1 + \left[m_2\frac{l_2^2}{4} + I_2 + m_2 l_1 l_2\cos(\theta_2)\right]\dot{\theta}_2\\ &\quad + \left[m_3\frac{l_3^2}{4} + I_3 + m_3 l_1 l_3\cos(\theta_3)\right]\ddot{\theta}_3 + \left[-m_2 l_1 l_2\sin(\theta_2)\dot{\theta}_2\left(\dot{\theta}_1 + \frac{\dot{\theta}_2}{2}\right)\right.\end{aligned}$$

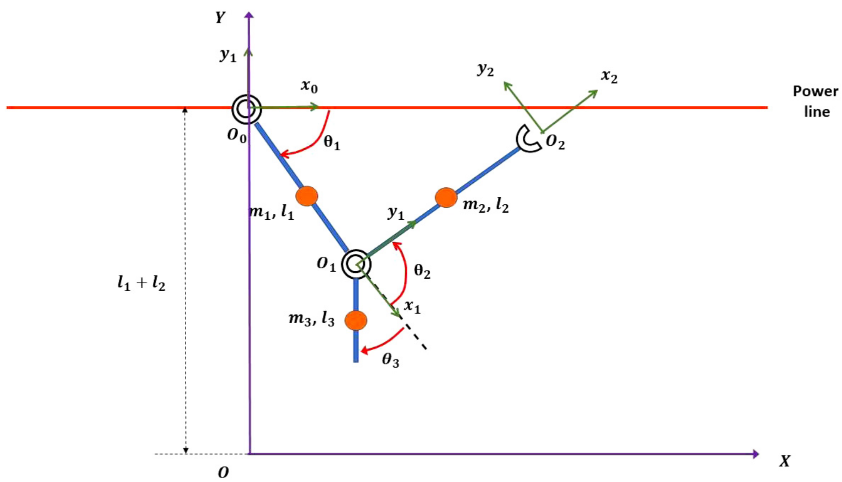

Fig. 1. Diagram of the multi-DOF brachiation robot.

$$
\begin{aligned}
&- m_3 l_1 l_3 \sin(\theta_3)\dot{\theta}_3\left(\dot{\theta}_1 + \frac{\dot{\theta}_3}{2}\right)\Bigg] + \left[m_1 g\frac{l_2}{2}\cos(\theta_1) + m_2 g l_1 \cos(\theta_2)\right.\\
&\left. + m_2 g \frac{l_2}{2}\cos(\theta_1+\theta_2) + m_3 g l_1 \cos(\theta_1) + [m_3] g \frac{l_2}{2}\cos(\theta_1+\theta_3)\right] + b_1\dot{\theta}_1 = T_1,
\end{aligned}
\tag{2}
$$

$$
\begin{aligned}
&\left[m_2\frac{l_2^2}{4} + m_2 l_1 l_2 \cos(\theta_2) + I_2\right]\ddot{\theta}_1 + \left[m_2\frac{l_2^2}{4} + I_2\right]\ddot{\theta}_2\\
&\qquad - m_2 l_1 l_2 \sin(\theta_1)\dot{\theta}_1\dot{\theta}_2 - m_2 g\frac{l_2}{2}\cos(\theta_1+\theta_2) + b_2\dot{\theta}_2 = T_2,
\end{aligned}
\tag{3}
$$

$$
\begin{aligned}
&\left[m_3\frac{l_3^2}{4} + m_3 l_1 l_3 \cos(\theta_3) + I_3\right]\ddot{\theta}_1 + \left[m_3\frac{l_3^2}{4} + I_3\right]\ddot{\theta}_3\\
&\qquad - m_3 l_1 l_3 \sin(\theta_1)\dot{\theta}_1\dot{\theta}_3 - m_3 g\frac{l_3}{2}\cos(\theta_1+\theta_3) + b_3\dot{\theta}_3 = 0.
\end{aligned}
\tag{4}
$$

Equivalently, the dynamic model of the brachiation robot can be written in the following matrix form:

$$
\begin{pmatrix} m_{11} & m_{12} & m_{13}\\ m_{21} & m_{22} & m_{23}\\ m_{31} & m_{32} & m_{33}\end{pmatrix}
\begin{pmatrix}\ddot{\theta}_1\\ \ddot{\theta}_2\\ \ddot{\theta}_3\end{pmatrix}
+ \begin{pmatrix} C_1(\theta,\dot{(\theta)})\\ C_2(\theta,\dot{(\theta)})\\ C_3(\theta,\dot{(\theta)})\end{pmatrix}
+ \begin{pmatrix} G_1(\theta)\\ G_2(\theta)\\ G_3(\theta)\end{pmatrix}
+ \begin{pmatrix} F_{v_1}\\ F_{v_2}\\ F_{v_3}\end{pmatrix}
= \begin{pmatrix} T_1\\ T_2\\ 0\end{pmatrix},
\tag{5}
$$

where

$$
\begin{aligned}
m_{11} &= \left[m_1\frac{l_1^2}{2} + I_1 + m_2 l_1^2 + m_2\frac{l_2^2}{4} + I_2 + m_3 l_1^2 + m_3\frac{l_3^2}{4} + m_2 l_1 l_2\cos(\theta_2) + I_3\right.\\
&\quad\left. + m_3 l_1 l_3 \cos(\theta_3)\right],\\
m_{12} &= \left[m_2\frac{l_2^2}{4} + I_2 + m_2 l_1 l_2 \cos(\theta_2)\right], \quad m_{13} = \left[m_3\frac{l_3^2}{4} + I_3 + m_3 l_1 l_3\cos(\theta_3)\right],\\
m_{21} &= \left[m_2\frac{l_2^2}{4} + I_2 + m_2 l_1 l_2 \cos(\theta_2)\right], \quad m_{22} = \left[m_2\frac{l_2^2}{4} + I_2\right], \quad m_{23} = 0,\\
m_{31} &= \left[m_3\frac{l_3^2}{4} + m_3 l_1 l_3 \cos(\theta_3) + I_3\right], \quad m_{32} = 0, \quad m_{33} = \left[m_3\frac{l_3^2}{4} + I_3\right].
\end{aligned}
$$

Besides, the elements of the Coriolis forces matrix $C(\theta,\dot{\theta})$ are given by

$$
\begin{aligned}
C_1(\theta,\dot{\theta}) &= \left[-m_2 l_1 l_2 \sin(\theta_2)\dot{\theta}_2\left(\dot{\theta}_1 + \frac{\dot{\theta}_2}{2}\right) - m_3 l_1 l_3 \sin(\theta_3)\dot{\theta}_3\left(\dot{\theta}_1 + \frac{\dot{\theta}_3}{2}\right)\right],\\
C_2(\theta,\dot{\theta}) &= - m_2 l_1 l_2 \sin(\theta_1)\dot{\theta}_1\dot{\theta}_2, \quad \text{and} \quad C_3(\theta,\dot{\theta}) = -m_3 l_1 l_3 \sin(\theta_1)\dot{\theta}_1\dot{\theta}_3.
\end{aligned}
$$

About the elements of the gravitational forces vector one has

$$\begin{aligned} G_1(\theta) = & \left[m_1 g \frac{l_2}{2} \cos(\theta_1) + m_2 g l_1 \cos(\theta_2) + m_2 g \frac{l_2}{2} \cos(\theta_1 + \theta_2) + m_3 g l_1 \cos(\theta_1) \right. \\ & \left. + [m_3] g \frac{l_2}{2} \cos(\theta_1 + \theta_3) \right], \\ G_2(\theta) = & - m_2 g \frac{l_2}{2} \cos(\theta_1 + \theta_2) \quad \text{and} \quad G_3(\theta) = -m_3 g \frac{l_3}{2} \cos(\theta_1 + \theta_3). \end{aligned}$$

While the elements of the friction torques vector $F_v(\theta)$ are given by

$$F_{v_1}(\dot{\theta}) = b_1 \dot{\theta}_1, \quad F_{v_2}(\dot{\theta}) = b_2 \dot{\theta}_2 \quad \text{and} \quad F_{v_3}(\dot{\theta}) = b_3 \dot{\theta}_3.$$

Finally, the control input torques vector τ is given by $\tau = [T_1, T_2, 0]^T$, which denotes that the brachiation robot functions in the underactuation mode. Next, the inverse of the inertia matrix M is computed as follows:

$$M^{-1} = \frac{1}{\det M} \begin{pmatrix} M_{11} & -M_{21} & M_{31} \\ -M_{12} & M_{22} & -M_{32} \\ M_{13} & -M_{23} & M_{33} \end{pmatrix}, \tag{6}$$

where using that $m_{23} = 0$ and $m_{32} = 0$, the determinant $\det M$ is

$$\begin{aligned} \det M = & \, m_{11}(m_{22} m_{33} - m_{32} m_{23}) - m_{12}(m_{21} m_{33} - m_{23} m_{31}) \\ & + m_{13}(m_{21} m_{32} - m_{31} m_{22}) \\ \Rightarrow \det M = & \, m_{11} m_{22} m_{33} - m_{12} m_{21} m_{33} - m_{13} m_{31} m_{22}, \end{aligned} \tag{7}$$

while it also holds that $M_{11} = m_{22} m_{33}$, $M_{12} = m_{21} m_{33}$, $M_{13} = -m_{31} m_{22}$, $M_{21} = m_{12} m_{33}$, $M_{22} = m_{11} m_{33} - m_{31} m_{13}$, $M_{23} = -m_{31} m_{12}$, $M_{31} = -m_{22} m_{13}$, $M_{32} = -m_{21} m_{13}$, $M_{33} = m_{11} m_{22} - m_{21} m_{12}$.

The state-space model of the robotic system is written as

$$\ddot{\theta} = -M^{-1}(\theta) C(\theta, \dot{\theta}) - M^{-1}(\theta) G(\theta) - M^{-1}(\theta) F_v(\dot{\theta}) + M^{-1}(\theta)\tau. \tag{8}$$

After intermediate operations, the state-space model of the brachiation robot takes the form

$$\begin{pmatrix} \ddot{\theta}_1 \\ \ddot{\theta}_2 \\ \ddot{\theta}_3 \end{pmatrix} = \begin{pmatrix} \dfrac{\begin{array}{c} -(M_{11} C_1 - M_{21} C_2 + M_{31} C_3) - (M_{11} G_1 - M_{21} G_2 + M_{31} G_3) \\ - (M_{11} F_{v1} - M_{21} F_{v2} + M_{31} F_{v3}) \end{array}}{\det M} \\ \dfrac{\begin{array}{c} -(-M_{12} C_1 + M_{22} C_2 - M_{32} C_3) - (-M_{12} G_1 + M_{22} G_2 - M_{32} G_3) \\ - (-M_{12} F_{v1} + M_{22} F_{v2} - M_{32} F_{v3}) \end{array}}{\det M} \\ \dfrac{\begin{array}{c} -(M_{13} C_1 - M_{23} C_2 + M_{33} C_3) - (M_{13} G_1 - M_{23} G_2 + M_{33} G_3) \\ - (M_{13} F_{v1} - M_{23} F_{v2} + M_{33} F_{v3}) \end{array}}{\det M} \end{pmatrix}$$

$$+\begin{pmatrix} \dfrac{M_{11}}{\det M} \\ -\dfrac{M_{12}}{\det M} \\ \dfrac{M_{13}}{\det M} \end{pmatrix} T_1 + \begin{pmatrix} \dfrac{-M_{21}}{\det M} \\ \dfrac{M_{22}}{\det M} \\ \dfrac{-M_{23}}{\det M} \end{pmatrix} T_2. \tag{9}$$

Next, the following state variables are defined: $x_1 = \theta_1$, $x_2 = \dot{\theta}_1$, $x_3 = \theta_2$, $x_4 = \dot{\theta}_2$, $x_5 = \theta_3$, $x_6 = \dot{\theta}_3$. Moreover, the following control input variables are defined: $u_1 = T_1$ and $u_2 = T_2$.

Thus, about the elements of the inertia matrix M it holds:

$$\begin{aligned} m_{11}(x) = {} & \left[m_1 \frac{l_1^2}{2} + I_1 + m_2 l_1^2 + m_2 \frac{l_2^2}{4} + I_2 + m_3 l_1^2 + m_3 \frac{l_3^2}{4} + m_2 l_1 l_2 \cos(x_3) \right. \\ & \left. + \, I_3 + m_3 l_1 l_3 \cos(x_5) \right], \\ m_{12}(x) = {} & \left[m_2 \frac{l_2^2}{4} + I_2 + m_2 l_1 l_2 \cos(x_3)\right], \quad m_{13}(x) = \left[m_3 \frac{l_3^2}{4} + I_3 + m_3 l_1 l_3 \cos(x_5)\right], \\ m_{21}(x) = {} & \left[m_2 \frac{l_2^2}{4} + I_2 + m_2 l_1 l_2 \cos(x_3)\right], \quad m_{22}(x) = \left[m_2 \frac{l_2^2}{4} + I_2\right], \quad m_{23}(x) = 0, \\ m_{31}(x) = {} & \left[m_3 \frac{l_3^2}{4} + m_3 l_1 l_3 \cos(x_5) + I_3\right], \quad m_{32}(x) = 0, \quad m_{33}(x) = \left[m_3 \frac{l_3^2}{4} + I_3\right]. \end{aligned}$$

where the determinant is

$$\det M = m_{11}(x) m_{22}(x) m_{33}(x) - m_{12}(x) m_{21}(x) m_{33}(x) - m_{13}(x) m_{31}(x) m_{22}(x). \tag{10}$$

In particular, it holds that $M_{11} = m_{22}(x) m_{33}(x)$, $M_{12} = m_{21}(x) m_{33}(x)$, $M_{13} = -m_{31}(x) m_{22}(x)$, $M_{21} = m_{12}(x) m_{33}(x)$, $M_{22} = m_{11}(x) m_{33}(x) - m_{31}(x) m_{13}(x)$, $M_{23} = -m_{31}(x) m_{12}(x)$, $M_{31} = -m_{22}(x) m_{13}(x)$, $M_{32} = -m_{21}(x) m_{13}(x)$, $M_{33} = m_{11}(x) m_{22}(x) - m_{21}(x) m_{12}(x)$.

Besides, the elements of the Coriolis forces matrix C are given by

$$\begin{aligned} C_1 = & -\left[m_2 l_1 l_2 \sin(x_3) x_4 \left(x_2 + \frac{x_4}{2}\right) - m_3 l_1 l_3 \sin(x_5) x_6 \left(x_2 + \frac{x_6}{2}\right)\right], \\ C_2 = & -m_2 l_1 l_2 \sin(x_3) x_2 x_4, \quad \text{and} \quad C_3 = -m_3 l_1 l_3 \sin(x_5) x_2 x_6. \end{aligned}$$

About the elements of the gravitational forces vector one has

$$\begin{aligned} G_1 = {} & \left[m_1 g \frac{l_2}{2} \cos(x_1) + m_2 g l_1 \cos(x_3) + m_2 g \frac{l_2}{2} \cos(x_1 + x_3) + m_3 g l_1 \cos(x_1) \right. \\ & \left. + \, [m_3] g \frac{l_2}{2} \cos(x_1 + x_5) \right], \\ G_2 = {} & -m_2 g l_2 2 \cos(x_1 + x_3) \quad \text{and} \quad G_3 = -m_3 g \frac{l_3}{2} \cos(x_1 + x_5). \end{aligned}$$

While the elements of the friction torques vector $F_v(\theta)$ are given by $F_{v_1} = b_1 x_2$, $F_{v_2} = b_2 x_4$ and $F_{v_3} = b_3 x_5$.

Finally, the state-space model of the brachiation robot is written in a form that comprises the following equations:

$$\dot{x}_1 = x_2, \tag{11}$$

$$\begin{aligned}\dot{x}_2 = {} & \frac{\begin{array}{l}-(M_{11}C_1 - M_{21}C_2 + M_{31}C_3) - (M_{11}G_1 - M_{21}G_2 + M_{31}G_3)\\ \quad - (M_{11}F_{v1} - M_{21}F_{v2} + M_{31}F_{v3})\end{array}}{\det M}\\ & + \frac{M_{11}}{\det M}T_1 + \frac{-M_{21}}{\det M}T_2,\end{aligned} \tag{12}$$

$$\dot{x}_3 = x_4, \tag{13}$$

$$\begin{aligned}\dot{x}_4 = {} & \frac{\begin{array}{l}-(-M_{12}C_1 + M_{22}C_2 - M_{32}C_3) - (-M_{12}G_1 + M_{22}G_2 - M_{32}G_3)\\ \quad - (-M_{12}F_{v1} + M_{22}F_{v2} - M_{32}F_{v3})\end{array}}{\det \mathrm{M}}\\ & + \frac{-M_{12}}{\det M}T_1 + \frac{M_{22}}{\det M}T_2,\end{aligned} \tag{14}$$

$$\dot{x}_5 = x_6, \tag{15}$$

$$\begin{aligned}\dot{x}_6 = {} & \frac{\begin{array}{l}-(M_{13}C_1 - M_{23}C_2 + M_{33}C_3) - (M_{13}G_1 - M_{23}G_2 + M_{33}G_3)\\ \quad - (M_{13}F_{v1} - M_{23}F_{v2} + M_{33}F_{v3})\end{array}}{\det M}\\ & + \frac{M_{13}}{\det M}T_1 + \frac{-M_{23}}{\det M}T_2.\end{aligned} \tag{16}$$

Thus, the state-space model of the brachiation robot is written in the following concise matrix form:

$$\dot{x} = f(x) + g_1(x)u_1 + g_2(x)u_2, \tag{17}$$

where $x \in R^{6\times 1}$, $f(x) \in R^{6\times 1}$, $g(x) \in R^{6\times 1}$, and $u \in R^{2\times 1}$, where vectors $f(x)$ and $g(x)$ are given by

$$f(x) = \begin{pmatrix} x_2 \\ \dfrac{\begin{array}{l}-(M_{11}C_1 - M_{21}C_2 + M_{31}C_3) - (M_{11}G_1 - M_{21}G_2 + M_{31}G_3)\\ \quad - (M_{11}F_{v1} - M_{21}F_{v2} + M_{31}F_{v3})\end{array}}{\det M} \\ x_4 \\ \dfrac{\begin{array}{l}-(-M_{12}C_1 + M_{22}C_2 - M_{32}C_3) - (-M_{12}G_1 + M_{22}G_2 - M_{32}G_3)\\ \quad - (-M_{12}F_{v1} + M_{22}F_{v2} - M_{32}F_{v3})\end{array}}{\det M} \\ x_6 \\ \dfrac{\begin{array}{l}-(M_{13}C_1 - M_{23}C_2 + M_{33}C_3) - (M_{13}G_1 - M_{23}G_2 + M_{33}G_3)\\ \quad - (M_{13}F_{v1} - M_{23}F_{v2} + M_{33}F_{v3})\end{array}}{\det M} \end{pmatrix}, \tag{18}$$

$$g_1(x) = \begin{pmatrix} 0 \\ \frac{M_{11}}{\det M} \\ 0 \\ \frac{-M_{12}}{\det M} \\ 0 \\ \frac{M_{13}}{\det M} \end{pmatrix}, \quad g_2(x) = \begin{pmatrix} 0 \\ \frac{-M_{21}}{\det M} \\ 0 \\ \frac{M_{22}}{\det M} \\ 0 \\ \frac{-M_{23}}{\det M} \end{pmatrix}. \tag{19}$$

3. Approximate Linearization of the Dynamic Model of the Brachiation Robot

3.1. *Approximate linearization of the robot's model*

The dynamic model of the brachiation robot undergoes approximate linearization around the time-varying operating point (x^*, u^*) which is updated at each iteration of the control algorithm, while x^* is the present value of the system's state vector and u^* is the last sampled value of the control inputs vector. The linearization process relies on first-order Taylor series expansion and on the computation of the related Jacobian matrices. Thus, the state-space model of the robot being initially in the form $\dot{x} = f(x) + g(x)u$, where $g(x) = [g_1(x), g_2(x)]$ is written in the linearized form

$$\dot{x} = Ax + Bu + \tilde{d}, \tag{20}$$

where $\tilde{d}$ is the cumulative vector of disturbances which may comprise (i) modeling error terms due to the truncation of higher-order terms in the Taylor series expansion, (ii) exogenous perturbations, (iii) measurement noise of any distribution. Matrices A and B are obtained from the system's Jacobians

$$\begin{aligned} & A = \nabla_x[f(x) + g(x)u]|_{(x^*,u^*)} \\ \Rightarrow\ & A = \nabla_x[f(x)]|_{(x^*,u^*)} + \nabla_x[g_1(x)]u_1|_{(x^*,u^*)} + \nabla_x[g_2(x)]u_2|_{(x^*,u^*)}, \end{aligned} \tag{21}$$

$$B = \nabla_u[f(x) + g(x)u]|_{(x^*,u^*)} \Rightarrow B = g(x)|_{(x^*,u^*)}. \tag{22}$$

Next, the computation of the Jacobian matrix $A = \nabla_x f(x)|_{(x^*,u^*)}$ is performed.

First row of the Jacobian matrix $\nabla_x f(x)|_{(x^*,u^*)}$: $\frac{\partial f_1}{\partial x_1} = 0$, $\frac{\partial f_1}{\partial x_2} = 1$, $\frac{\partial f_1}{\partial x_3} = 0$, $\frac{\partial f_1}{\partial x_4} = 0$, $\frac{\partial f_1}{\partial x_5} = 0$, $\frac{\partial f_1}{\partial x_6} = 0$, $\frac{\partial f_1}{\partial x_7} = 0$, and $\frac{\partial f_1}{\partial x_8} = 0$.

Second row of the Jacobian matrix $\nabla_x f(x)|_{(x^*,u^*)}$:

The numerator of $f_2(x)$ is

$$\begin{aligned} f_{2n} = & -(M_{11}C_1 - M_{21}C_2 + M_{31}C_3) - (M_{11}G_1 - M_{21}G_2 + M_{31}G_3) \\ & - (M_{11}F_{v1} - M_{21}F_{v2} + M_{31}F_{v3}), \end{aligned} \tag{23}$$

while the denominator of $f_2(x)$ is $f_{2d} = \det M$. It holds that for $i = 1, 2, \ldots, 6$

$$\begin{aligned}\frac{\partial f_{2n}}{\partial x_i} = &-\left(\frac{\partial M_{11}}{\partial x_i}C_1 + M_{11}\frac{\partial C_1}{\partial x_i} - \frac{\partial M_{21}}{\partial x_i}C_2 - M_{21}\frac{\partial C_2}{\partial x_i} + \frac{\partial M_{31}}{\partial x_i}C_3 + M_{31}\frac{\partial C_3}{\partial x_i}\right)\\ &-\left(\frac{\partial M_{11}}{\partial x_i}G_1 + M_{11}\frac{\partial G_1}{\partial x_i} - \frac{\partial M_{21}}{\partial x_i}G_2 - M_{21}\frac{\partial G_2}{\partial x_i} + \frac{\partial M_{31}}{\partial x_i}G_3 + M_{31}\frac{\partial G_3}{\partial x_i}\right)\\ &-\left(\frac{\partial M_{11}}{\partial x_i}F_{v1} + M_{11}\frac{\partial F_{v1}}{\partial x_i} - \frac{\partial M_{21}}{\partial x_i}F_{v2} - M_{21}\frac{\partial F_{v2}}{\partial x_i} + \frac{\partial M_{31}}{\partial x_i}F_{v3} + M_{31}\frac{\partial F_{v3}}{\partial x_i}\right).\end{aligned} \tag{24}$$

Moreover, for $i = 1, 2, \ldots, 6$, one obtains that

$$\frac{\partial f_{2d}}{\partial x_i} = \frac{\partial \det M}{\partial x_i}. \tag{25}$$

Therefore, for the second row of the Jacobian matrix

$$\frac{\partial f_2}{\partial x_i} = \frac{\frac{\partial f_{2n}}{\partial x_i} f_{2d} - f_{2n}\frac{\partial f_{2d}}{\partial x_i}}{\det M^2}. \tag{26}$$

Third row of the Jacobian matrix $\nabla_x f(x)|_{(x^*,u^*)}$: $\frac{\partial f_3}{\partial x_1} = 0$, $\frac{\partial f_3}{\partial x_2} = 0$, $\frac{\partial f_3}{\partial x_3} = 0$, $\frac{\partial f_3}{\partial x_4} = 0$, $\frac{\partial f_3}{\partial x_5} = 0$, $\frac{\partial f_3}{\partial x_6} = 0$, $\frac{\partial f_3}{\partial x_7} = 0$, and $\frac{\partial f_3}{\partial x_8} = 0$.

Fourth row of the Jacobian matrix $\nabla_x f(x)|_{(x^*,u^*)}$:

The numerator of $f_4(x)$ is

$$\begin{aligned}f_{4n} = &-(-M_{12}C_1 + M_{22}C_2 - M_{32}C_3) - (-M_{12}G_1 + M_{22}G_2 - M_{32}G_3)\\ &-(-M_{12}F_{v1} + M_{22}F_{v2} - M_{32}F_{v3}),\end{aligned} \tag{27}$$

while the denominator of $f_4(x)$ is $f_{4d} = \det M$. It holds that for $i = 1, 2, \ldots, 6$

$$\begin{aligned}\frac{\partial f_{4n}}{\partial x_i} = &-\left(-\frac{\partial M_{12}}{\partial x_i}C_1 - M_{12}\frac{\partial C_1}{\partial x_1} + \frac{\partial M_{22}}{\partial x_i}C_2 + M_{22}\frac{\partial C_2}{\partial x_i} - \frac{\partial M_{32}}{\partial x_i}C_3 - M_{32}\frac{\partial C_3}{\partial x_i}\right)\\ &-\left(-\frac{\partial M_{12}}{\partial x_i}G_1 - M_{12}\frac{\partial G_1}{\partial x_i} + \frac{\partial M_{22}}{\partial x_i}G_2 + M_{22}\frac{\partial G_2}{\partial x_i} - \frac{\partial M_{32}}{\partial x_i}G_3 - M_{32}\frac{\partial G_3}{\partial x_i}\right)\\ &-\left(\frac{\partial M_{12}}{\partial x_i}F_{v1} - M_{12}\frac{\partial F_{v1}}{\partial x_i} + \frac{\partial M_{22}}{\partial x_i}F_{v2} + M_{22}\frac{\partial F_{v2}}{\partial x_i} - \frac{\partial M_{32}}{\partial x_i}F_{v3} - M_{32}\frac{\partial F_{v3}}{\partial x_i}\right).\end{aligned} \tag{28}$$

Moreover, for $i = 1, 2, \ldots, 6$, one obtains that

$$\frac{\partial f_{4d}}{\partial x_i} = \frac{\partial \det M}{\partial x_i}. \tag{29}$$

Therefore, for the fourth row of the Jacobian matrix

$$\frac{\partial f_4}{\partial x_i} = \frac{\frac{\partial f_{4n}}{\partial x_i} f_{4d} - f_{4n}\frac{\partial f_{4d}}{\partial x_i}}{\det M^2}. \tag{30}$$

Fifth row of the Jacobian matrix $\nabla_x f(x)|_{(x^*,u^*)}$: $\frac{\partial f_5}{\partial x_1} = 0$, $\frac{\partial f_5}{\partial x_2} = 0$, $\frac{\partial f_5}{\partial x_3} = 0$, $\frac{\partial f_5}{\partial x_4} = 0$, $\frac{\partial f_5}{\partial x_5} = 0$, $\frac{\partial f_5}{\partial x_6} = 0$, $\frac{\partial f_5}{\partial x_7} = 0$, and $\frac{\partial f_5}{\partial x_8} = 0$.

Sixth row of the Jacobian matrix $\nabla_x f(x)|_{(x^*,u^*)}$:
The numerator of $f_6(x)$ is

$$\begin{aligned} f_{6n} = & -(M_{13}C_1 - M_{23}C_2 + M_{33}C_3) - (M_{13}G_1 - M_{23}G_2 + M_{33}G_3) \\ & -(M_{13}F_{v1} - M_{23}F_{v2} + M_{33}F_{v3}), \end{aligned} \tag{31}$$

while the denominator of $f_4(x)$ is $f_{4d} = \det M$. It holds that for $i = 1, 2, \ldots, 6$

$$\begin{aligned} \frac{\partial f_{6n}}{\partial x_i} = & -\left(-\frac{\partial M_{13}}{\partial x_i}C_1 - M_{13}\frac{\partial C_1}{\partial x_1} + \frac{\partial M_{23}}{\partial x_i}C_2 + M_{23}\frac{\partial C_2}{\partial x_i} - \frac{\partial M_{33}}{\partial x_i}C_3 - M_{33}\frac{\partial C_3}{\partial x_i}\right) \\ & -\left(-\frac{\partial M_{13}}{\partial x_i}G_1 - M_{13}\frac{\partial G_1}{\partial x_i} + \frac{\partial M_{23}}{\partial x_i}G_2 + M_{23}\frac{\partial G_2}{\partial x_i} - \frac{\partial M_{33}}{\partial x_i}G_3 - M_{33}\frac{\partial G_3}{\partial x_i}\right) \\ & -\left(\frac{\partial M_{13}}{\partial x_i}F_{v1} - M_{13}\frac{\partial F_{v1}}{\partial x_i} + \frac{\partial M_{23}}{\partial x_i}F_{v2} + M_{23}\frac{\partial F_{v2}}{\partial x_i} - \frac{\partial M_{33}}{\partial x_i}F_{v3} - M_{33}\frac{\partial F_{v3}}{\partial x_i}\right). \end{aligned} \tag{32}$$

Moreover, for $i = 1, 2, \ldots, 6$, one obtains that

$$\frac{\partial f_{6d}}{\partial x_i} = \frac{\partial \det M}{\partial x_i}. \tag{33}$$

Therefore, for the sixth row of the Jacobian matrix

$$\frac{\partial f_6}{\partial x_i} = \frac{\frac{\partial f_{6n}}{\partial x_i} f_{6d} - f_{6n}\frac{\partial f_{6d}}{\partial x_i}}{\det M^2}. \tag{34}$$

Next, the computation of the Jacobian matrix $\nabla_x g_1(x)|_{(x^*,u^*)}$ is performed.

For the first row of the Jacobian matrix and for $i = 1, 2, \ldots, 6$ it holds

$$\frac{\partial g_{11}}{\partial x_i} = 0. \tag{35}$$

For the second row of the Jacobian matrix and for $i = 1, 2, \ldots, 6$ it holds

$$\frac{\partial g_{21}}{\partial x_i} = \frac{\frac{\partial M_{11}}{\partial x_i}\det M - M_{11}\frac{\partial \det M}{\partial x_i}}{\det M^2}. \tag{36}$$

For the third row of the Jacobian matrix and for $i = 1, 2, \ldots, 6$ it holds

$$\frac{\partial g_{31}}{\partial x_i} = 0. \tag{37}$$

For the fourth row of the Jacobian matrix and for $i = 1, 2, \ldots, 6$ it holds

$$\frac{\partial g_{41}}{\partial x_i} = \frac{\frac{\partial M_{12}}{\partial x_i}\det M - M_{12}\frac{\partial \det M}{\partial x_i}}{\det M^2}. \tag{38}$$

For the fifth row of the Jacobian matrix and for $i = 1, 2, \ldots, 6$ it holds

$$\frac{\partial g_{51}}{\partial x_i} = 0. \tag{39}$$

For the sixth row of the Jacobian matrix and for $i = 1, 2, \ldots, 6$ it holds

$$\frac{\partial g_{61}}{\partial x_i} = \frac{\frac{\partial M_{13}}{\partial x_i}\,\mathrm{det}M - M_{13}\frac{\partial\,\mathrm{det}M}{\partial x_i}}{\mathrm{det}M^2}. \tag{40}$$

Additionally, the computation of the Jacobian matrix $\nabla_x g_2(x)|_{(x^*,u^*)}$ is performed.

For the first row of the Jacobian matrix and for $i = 1, 2, \ldots, 6$ it holds

$$\frac{\partial g_{12}}{\partial x_i} = 0. \tag{41}$$

For the second row of the Jacobian matrix and for $i = 1, 2, \ldots, 6$ it holds

$$\frac{\partial g_{22}}{\partial x_i} = \frac{\frac{\partial M_{21}}{\partial x_i}\,\mathrm{det}M - M_{21}\frac{\partial\,\mathrm{det}M}{\partial x_i}}{\mathrm{det}\,M^2}. \tag{42}$$

For the third row of the Jacobian matrix and for $i = 1, 2, \ldots, 6$ it holds

$$\frac{\partial g_{33}}{\partial x_i} = 0. \tag{43}$$

For the fourth row of the Jacobian matrix and for $i = 1, 2, \ldots, 6$ it holds

$$\frac{\partial g_{42}}{\partial x_i} = \frac{\frac{\partial M_{22}}{\partial x_i}\,\mathrm{det}M - M_{22}\frac{\partial\,\mathrm{det}M}{\partial x_i}}{\mathrm{det}\,M^2}. \tag{44}$$

For the fifth row of the Jacobian matrix and for $i = 1, 2, \ldots, 6$ it holds

$$\frac{\partial g_{52}}{\partial x_i} = 0. \tag{45}$$

For the sixth row of the Jacobian matrix and for $i = 1, 2, \ldots, 6$ it holds

$$\frac{\partial g_{62}}{\partial x_i} = \frac{\frac{\partial M_{23}}{\partial x_i}\,\mathrm{det}M - M_{33}\frac{\partial\,\mathrm{det}M}{\partial x_i}}{\mathrm{det}M^2}. \tag{46}$$

Next, one computes the partial derivatives of the elements of the inertia matrix M, of the Coriolis and centrifugal terms matrix C, of the gravitational terms matrix G and of the viscous friction terms matrix F_v. It holds that

$$\frac{\partial M_{11}}{\partial x_i} = 0 \quad \text{for } i = 1, \ldots, 6,$$

$$\frac{\partial M_{12}}{\partial x_3} = [-m_2 l_1 l_2 \sin(x_3)]\left[m_3\frac{l_3^2}{4} + I_3\right] \quad \text{and} \quad \frac{\partial M_{12}}{\partial x_i} = 0 \quad \text{for } i = 1, 2, 4, 5, 6,$$

$$\frac{\partial M_{13}}{\partial x_5} = [m_3 l_1 l_3 \sin(x_5)]\left[m_2\frac{l_2^2}{4} + I_2\right] \quad \text{and} \quad \frac{\partial M_{13}}{\partial x_i} = 0 \quad \text{for } i = 1, 2, 3, 4, 6,$$

$$\frac{\partial M_{21}}{\partial x_3} = [-m_2 l_1 l_2 \sin(x_3)]\left[m_3\frac{l_3^2}{4} + I_3\right] \quad \text{and} \quad \frac{\partial M_{21}}{\partial x_i} = 0 \quad \text{for } i = 1, 2, 4, 5, 6,$$

$$\frac{\partial M_{22}}{\partial x_i} = 0 \quad \text{for } i = 1,2,4,6, \quad \frac{\partial M_{22}}{\partial x_3} = [-m_2 l_1 l_2 \sin(x_3)]\left[m_3 \frac{l_3^2}{4} + I_3\right],$$
$$\frac{\partial M_{22}}{\partial x_5} = [-m_3 l_1 l_3 \sin(x_6)]\left[m_3 \frac{l_3^2}{4} + I_3\right] - 2\left[m_3 \frac{l_3^2}{4} + I_3 + m_3 l_1 l_3 \cos(x_5)\right] \times [-m_3 l_1 l_3 \sin(x_5)],$$

$$\frac{\partial M_{23}}{\partial x_3} = \left[m_3 \frac{l_3^2}{4} + I_3 + m_3 l_1 l_3 \cos(x_5)\right][m_2 l_1 l_2 \sin(x_3)],$$
$$\frac{\partial M_{23}}{\partial x_5} = \left[m_2 \frac{l_2^2}{4} + I_2 + m_2 l_1 l_2 \cos(x_3)\right][m_3 l_1 l_3 \sin(x_5)], \quad \text{and}$$
$$\frac{\partial M_{23}}{\partial x_i} = 0 \quad \text{for } i = 1,2,4,6,$$

$$\frac{\partial M_{31}}{\partial x_5} = [m_3 l_1 l_3 \sin(x_5)]\left[m_2 \frac{l_2^2}{4} + I_2\right] \quad \text{and} \quad \frac{\partial M_{31}}{\partial x_i} = 0 \quad \text{for } i = 1,2,3,4,6,$$
$$\frac{\partial M_{32}}{\partial x_3} = \left[m_3 \frac{l_3^2}{4} + I_3 + m_3 l_1 l_3 \cos(x_5)\right][m_2 l_1 l_2 \sin(x_3)],$$
$$\frac{\partial M_{32}}{\partial x_5} = \left[m_2 \frac{l_2^2}{4} + I_2 + m_2 l_1 l_2 \cos(x_3)\right][m_3 l_1 l_3 \sin(x_5)] \quad \text{and}$$
$$\frac{\partial M_{32}}{\partial x_i} = 0 \quad \text{for } i = 1,2,4,6,$$
$$\frac{\partial M_{33}}{\partial x_i} = 0 \quad \text{for } i = 1,2,4,6, \quad \frac{\partial M_{33}}{\partial x_3} = [-m_2 l_1 l_2 \sin(x_3)]\left[m_2 \frac{l_2^2}{4} + I_2\right] - 2\left[m_2 \frac{l_2^2}{4} + I_2 + m_2 l_1 l_2 \cos(x_3)\right][-m_2 l_1 l_2 \sin(x_3)]$$
$$\frac{\partial M_{33}}{\partial x_5} = [-m_3 l_1 l_3 \sin(x_5)]\left[m_2 \frac{l_2^2}{4} + I_2\right],$$

$$\frac{\partial \det M}{\partial x_3} = [-m_2 l_1 l_2 \sin(x_3)]\left[m_2 \frac{l_2^2}{4} + I_2\right]\left[m_3 \frac{l_3^2}{4} + I_3\right] + 2\left[m_2 \frac{l_2^2}{4} + I_2 + m_2 l_1 l_2 \cos(x_3)\right][m_2 l_1 l_2 \sin(x_3)]\left[m_3 \frac{l_3^2}{4} + I_3\right],$$
$$\frac{\partial \det M}{\partial x_5} = [-m_3 l_1 l_3 \sin(x_5)]\left[m_2 \frac{l_2^2}{4} + I_2\right]\left[m_2 \frac{l_2^2}{4} + I_2\right] + 2\left[m_3 \frac{l_3^2}{4} + I_3 + m_3 l_1 l_3 \cos(x_5)\right][m_3 l_1 l_3 \sin(x_5)]\left[m_2 \frac{l_2^2}{4} + I_2\right],$$
$$\frac{\partial \det M}{\partial x_i} = 0 \quad \text{for } i = 1,2,4,6.$$

Moreover, it holds that

$$\begin{aligned}
&\frac{\partial C_1}{\partial x_1}=0, \quad \frac{\partial C_1}{\partial x_2}=-m_2 l_1 l_2 \sin(x_3)x_4 - m_3 l_1 l_3 \sin(x_5)x_6,\\
&\frac{\partial C_1}{\partial x_3}= -\, m_2 l_1 l_2 \cos(x_3)x_4\left(x_2+\frac{x_4}{2}\right),\\
&\frac{\partial C_1}{\partial x_4}= -\, m_2 l_1 l_2 \sin(x_3)\left(x_2+\frac{x_4}{2}\right) - m_2 l_1 l_2 \sin(x_3)\frac{x_4}{2},\\
&\frac{\partial C_1}{\partial x_5}= -\, m_3 l_1 l_3 \cos(x_5)x_6\left(x_2+\frac{x_6}{2}\right),\\
&\frac{\partial C_1}{\partial x_6}= -\, m_3 l_1 l_3 \sin(x_5)\left(x_2+\frac{x_6}{2}\right) - m_3 l_1 l_3 \sin(x_5)\frac{x_6}{2},\\
&\frac{\partial C_2}{\partial x_1}= -\, m_2 l_1 l_2 \sin(x_3)x_4, \quad \frac{\partial C_2}{\partial x_2}=0, \quad \frac{\partial C_2}{\partial x_3}=-m_2 l_1 l_2 \cos(x_3)x_2x_4,\\
&\frac{\partial C_2}{\partial x_4}= -\, m_2 l_1 l_2 \sin(x_3)x_2, \quad \frac{\partial C_1}{\partial x_5}=0, \quad \text{and} \quad \frac{\partial C_2}{\partial x_6}=0,\\
&\frac{\partial C_3}{\partial x_1}=0, \quad \frac{\partial C_3}{\partial x_2}=-m_3 l_1 l_3 \sin(x_5)x_6, \quad \frac{\partial C_3}{\partial x_3}=0, \quad \frac{\partial C_3}{\partial x_4}=0,\\
&\frac{\partial C_3}{\partial x_5}= -\, m_3 l_1 l_3 \cos(x_5)x_2x_6, \quad \text{and} \quad \frac{\partial C_3}{\partial x_6}=-m_3 l_1 l_3 \sin(x_5)x_2.
\end{aligned}$$

Furthermore, it holds that

$$\begin{aligned}
\frac{\partial G_1}{\partial x_1} &= -\, m_1 g\frac{l_2}{2}\sin(x_1) - m_3 g l_1 \sin(x_1) - m_2 g\frac{l_2}{2}\sin(x_1+x_3) - m_3 g l_1 \sin(x_1)\\
&\quad -\, m_3 g\frac{l_3}{2}\sin(x_1+x_3),\\
\frac{\partial G_1}{\partial x_2} &= 0, \quad \frac{\partial G_1}{\partial x_3}=-m_2 g\frac{l_2}{2}\sin(x_1+x_3), \quad \frac{\partial G_1}{\partial x_4}=0,\\
\frac{\partial G_1}{\partial x_5} &= -\, m_3 g\frac{l_3}{2}\sin(x_1+x_5), \quad \frac{\partial G_1}{\partial x_6}=0,\\
\frac{\partial G_2}{\partial x_1} &= m_2 g\frac{l_2}{2}\sin(x_1+x_3), \quad \frac{\partial G_2}{\partial x_2}=0, \quad \frac{\partial G_2}{\partial x_3}=m_2 g\frac{l_2}{2}\sin(x_1+x_3), \quad \frac{\partial G_2}{\partial x_4}=0,\\
\frac{\partial G_2}{\partial x_5} &= 0, \quad \text{and} \quad \frac{\partial G_2}{\partial x_6}=0,\\
\frac{\partial G_3}{\partial x_1} &= m_3 g\frac{l_3}{2}\sin(x_1+x_5), \quad \frac{\partial G_3}{\partial x_3}=0, \quad \frac{\partial G_3}{\partial x_4}=0,\\
\frac{\partial G_3}{\partial x_5} &= m_3 g\frac{l_3}{2}\sin(x_1+x_5), \quad \text{and} \quad \frac{\partial G_3}{\partial x_6}=0.
\end{aligned}$$

Additionally, it holds that

$$\frac{\partial F_{v1}}{\partial x_2}=b_1 \quad \text{and} \quad \frac{\partial F_{v1}}{\partial x_i}=0 \quad \text{for } i=1,3,4,5,6,$$

$$\frac{\partial F_{v2}}{\partial x_4} = b_2 \quad \text{and} \quad \frac{\partial F_{v2}}{\partial x_i} = 0 \quad \text{for } i = 1, 2, 3, 5, 6,$$
$$\frac{\partial F_{v3}}{\partial x_6} = b_3 \quad \text{and} \quad \frac{\partial F_{v2}}{\partial x_i} = 0 \quad \text{for } i = 1, 2, 3, 4, 5.$$

3.2. *Stabilizing feedback control*

After linearization around its current operating point, the dynamic model of the multi-DOF brachiation robot is written as[8]

$$\dot{x} = Ax + Bu + d_1. \tag{47}$$

Parameter d_1 stands for the linearization error in the multi-DOF brachiation robot dynamic model appearing in Eq. (47). The reference setpoints for the state vector of the multi-DOF brachiation robot are denoted by $\mathbf{x_d} = [x_1^d, \ldots, x_6^d]$. Tracking of this trajectory is achieved after applying the control input u^d. At every time instant the control input u^d is assumed to differ from the control input u appearing in Eq. (47) by an amount equal to Δu, that is, $u^d = u + \Delta u$

$$\dot{x}_d = Ax_d + Bu^d + d_2. \tag{48}$$

The dynamics of the controlled system described in Eq. (47) can be also written as

$$\dot{x} = Ax + Bu + Bu^d - Bu^d + d_1, \tag{49}$$

and by denoting $d_3 = -Bu^d + d_1$ as an aggregate disturbance term, one obtains

$$\dot{x} = Ax + Bu + Bu^d + d_3. \tag{50}$$

By subtracting Eq. (48) from Eq. (50), one has

$$\dot{x} - \dot{x}_d = A(x - x_d) + Bu + d_3 - d_2. \tag{51}$$

By denoting the tracking error as $e = x - x_d$ and the aggregate disturbance term as $\tilde{d} = d_3 - d_2$, the tracking error dynamics becomes

$$\dot{e} = Ae + Bu + \tilde{d}. \tag{52}$$

For the approximately linearized model of the system, a stabilizing feedback controller is developed. The controller has the form

$$u(t) = -Ke(t), \tag{53}$$

with $K = \frac{1}{r}B^T P$ where P is a positive definite symmetric matrix which is obtained from the solution of the Riccati equation[8]

$$A^T P + PA + Q - P\left(\frac{2}{r}BB^T - \frac{1}{\rho^2}LL^T\right)P = 0, \tag{54}$$

where Q is a positive semi-definite symmetric matrix. The diagram of the considered control loop is depicted in Fig. 2.

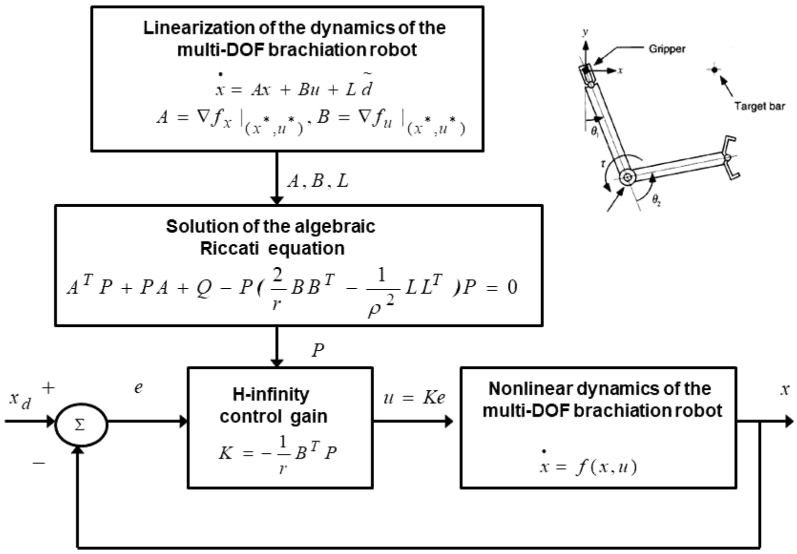

Fig. 2. Diagram of the nonlinear optimal (H-infinity) control loop for the multi-DOF brachiation robot.

The solution of the H-infinity feedback control problem for the multi-DOF brachiation robot and the computation of the worst-case disturbance that the related controller can sustain, comes from superposition of Bellman's optimality principle when considering that the robot is affected by two separate inputs (i) the control input u (ii) the cumulative disturbance input $\tilde{d}(t)$. Solving the optimal control problem for u, that is, for the minimum variation (optimal) control input that achieves elimination of the state vector's tracking error, gives $u = -\frac{1}{r} B^T Pe$. Equivalently, solving the optimal control problem for $\tilde{d}$, that is, for the worst-case disturbance that the control loop can sustain gives $\tilde{d} = \frac{1}{\rho^2} L^T Pe$.

A comparison of the proposed nonlinear optimal (H-infinity) control method against other linear and nonlinear control schemes for the multi-DOF brachiation robot's dynamics, shows the following:

(1) Unlike global linearization-based control approaches, such as Lie algebra-based control and differential flatness theory-based control, the optimal control approach does not rely on complicated transformations (diffeomorphisms) of the system's state variables. Besides, the computed control inputs are applied directly on the initial nonlinear model of the multi-DOF brachiation robot's dynamics and not on its linearized equivalent. The inverse transformations which are met in global linearization-based control are avoided, and consequently, one does not come against the related singularity problems.

(2) Unlike MPC and Nonlinear MPC (NMPC), the proposed control method is of proven global stability. It is known that MPC is a linear control approach that if applied to the nonlinear dynamics of the multi-DOF brachiation robot the

stability of the control loop will be lost. Besides, in NMPC the convergence of its iterative search for an optimum depends on initialization and parameter values selection, and consequently, the global stability of this control method cannot be always assured.

(3) Unlike sliding mode control and backstepping control the proposed optimal control method does not require the state-space description of the system to be found in a specific form. About sliding-mode control it is known that when the controlled system is not found in the input–output linearized form the definition of the sliding surface can be an intuitive procedure. About backstepping control it is known that it cannot be directly applied to a dynamical system if the related state-space model is not found in the triangular (backstepping integral) form.

(4) Unlike proportional integral derivative (PID) control, the proposed nonlinear optimal control method is of proven global stability, the selection of the controller's parameters does not rely on a heuristic tuning procedure, and the stability of the control loop is assured in the case of changes of operating points.

(5) Unlike multiple local models-based control the nonlinear optimal control method uses only one linearization point and needs the solution of only one Riccati equation so as to compute the stabilizing feedback gains of the controller. Consequently, in terms of computation load the proposed control method for the multi-DOF brachiation robot's dynamics is much more efficient.

4. Lyapunov Stability Analysis

4.1. *Proof of global stability properties*

Through Lyapunov stability analysis, it will be shown that the proposed nonlinear control scheme assures H_∞ tracking performance for the multi-DOF brachiation robot's dynamics, and that under moderate conditions asymptotic convergence to the reference setpoints (global stability) is achieved.[8] As shown before, the tracking error dynamics for the multi-DOF brachiation robot's dynamics is written in the form[8]

$$\dot{e} = Ae + Bu + L\tilde{d}, \tag{55}$$

where in the multi-DOF brachiation robot's case, $L = I \in R^{6\times 6}$ with I being the identity matrix. Variable $\tilde{d}$ denotes model uncertainties and external disturbances of the robotic manipulator's dynamic model. The following Lyapunov equation is considered:

$$V = \frac{1}{2}e^T Pe, \tag{56}$$

where $e = x - x_d$ is the tracking error. By differentiating with respect to time, one obtains

$$\begin{aligned}\dot{V} &= \frac{1}{2}\dot{e}^T Pe + \frac{1}{2}e^T P\dot{e} \Rightarrow \\ \dot{V} &= \frac{1}{2}[Ae + Bu + L\tilde{d}]^T Pe + \frac{1}{2}e^T P[Ae + Bu + L\tilde{d}] \Rightarrow\end{aligned} \tag{57}$$

$$\dot{V} = \frac{1}{2}[e^T A^T + u^T B^T + \tilde{d}^T L^T]Pe + \frac{1}{2}e^T P[Ae + Bu + L\tilde{d}] \Rightarrow \tag{58}$$

$$\dot{V} = \frac{1}{2}e^T A^T Pe + \frac{1}{2}u^T B^T Pe + \frac{1}{2}\tilde{d}^T L^T Pe + \frac{1}{2}e^T PAe + \frac{1}{2}e^T PBu + \frac{1}{2}e^T PL\tilde{d}. \tag{59}$$

The previous equation is rewritten as

$$\dot{V} = \frac{1}{2}e^T(A^T P + PA)e + \left(\frac{1}{2}u^T B^T Pe + \frac{1}{2}e^T PBu\right) + \left(\frac{1}{2}\tilde{d}^T L^T Pe + \frac{1}{2}e^T PL\tilde{d}\right). \tag{60}$$

Assumption: For the given positive definite matrix Q and coefficients r and ρ there exists a positive definite matrix P, which is the solution of the following matrix equation:

$$A^T P + PA = -Q + P\left(\frac{2}{r}BB^T - \frac{1}{\rho^2}LL^T\right)P. \tag{61}$$

Moreover, the following feedback control law is applied to the system:

$$u = -\frac{1}{r}B^T Pe. \tag{62}$$

By substituting Eqs. (61) and (62), one obtains

$$\dot{V} = \frac{1}{2}e^T\left[-Q + P\left(\frac{2}{r}BB^T - \frac{1}{2\rho^2}LL^T\right)P\right]e + e^T PB\left(-\frac{1}{r}B^T Pe\right) + e^T PL\tilde{d} \Rightarrow \tag{63}$$

$$\dot{V} = -\frac{1}{2}e^T Qe + \left(\frac{2}{r}e^T PBB^T Pe - \frac{1}{2\rho^2}e^T PLL^T Pe - \frac{1}{r}e^T PBB^T Pe\right) + e^T PL\tilde{d}, \tag{64}$$

which after intermediate operations gives

$$\dot{V} = -\frac{1}{2}e^T Qe - \frac{1}{2\rho^2}e^T PLL^T Pe + e^T PL\tilde{d}, \tag{65}$$

or, equivalently

$$\dot{V} = -\frac{1}{2}e^T Qe - \frac{1}{2\rho^2}e^T PLL^T Pe + \frac{1}{2}e^T PL\tilde{d} + \frac{1}{2}\tilde{d}^T L^T Pe. \tag{66}$$

Lemma: *The following inequality holds*:

$$\frac{1}{2}e^T PL\tilde{d} + \frac{1}{2}\tilde{d}L^T Pe - \frac{1}{2\rho^2}e^T PLL^T Pe \le \frac{1}{2}\rho^2\tilde{d}^T\tilde{d}. \tag{67}$$

Proof. The binomial $(\rho\alpha - \frac{1}{\rho}b)^2$ is considered. Expanding the left part of the above inequality, one gets

$$\rho^2 a^2 + \frac{1}{\rho^2}b^2 - 2ab \geq 0 \Rightarrow \frac{1}{2}\rho^2 a^2 + \frac{1}{2\rho^2}b^2 - ab \geq 0 \Rightarrow ab - \frac{1}{2\rho^2}b^2 \leq \frac{1}{2}\rho^2 a^2$$
$$\Rightarrow \frac{1}{2}ab + \frac{1}{2}ab - \frac{1}{2\rho^2}b^2 \leq \frac{1}{2}\rho^2 a^2. \tag{68}$$

The following substitutions are carried out: $a = \tilde{d}$ and $b = e^T PL$ and the previous relation becomes

$$\frac{1}{2}\tilde{d}^T L^T Pe + \frac{1}{2}e^T PL\tilde{d} - \frac{1}{2\rho^2}e^T PLL^T Pe \leq \frac{1}{2}\rho^2 \tilde{d}^T \tilde{d}. \tag{69}$$

Equation (69) is substituted in Eq. (66) and the inequality is enforced, thus giving

$$\dot{V} \leq -\frac{1}{2}e^T Qe + \frac{1}{2}\rho^2 \tilde{d}^T \tilde{d}. \tag{70}$$

Equation (70) shows that the H_∞ tracking performance criterion is satisfied. The integration of $\dot{V}$ from 0 to T gives

$$\int_0^T \dot{V}(t)dt \leq -\frac{1}{2}\int_0^T ||e||_Q^2 dt + \frac{1}{2}\rho^2 \int_0^T ||\tilde{d}||^2 dt \Rightarrow 2V(T) + \int_0^T ||e||_Q^2 dt$$
$$\leq 2V(0) + \rho^2 \int_0^T ||\tilde{d}||^2 dt. \tag{71}$$

Moreover, if there exists a positive constant $M_d > 0$ such that

$$\int_0^\infty ||\tilde{d}||^2 dt \leq M_d, \tag{72}$$

then, one gets

$$\int_0^\infty ||e||_Q^2 dt \leq 2V(0) + \rho^2 M_d. \tag{73}$$

Thus, the integral $\int_0^\infty ||e||_Q^2 dt$ is bounded. Moreover, $V(T)$ is bounded and from the definition of the Lyapunov function V in Eq. (56) it becomes clear that $e(t)$ will be also bounded since $e(t) \in \Omega_e = \{e | e^T Pe \leq 2V(0) + \rho^2 M_d\}$.

According to the above and with the use of Barbalat's Lemma, one obtains $\lim_{t\to\infty} e(t) = 0$.

The outline of the global stability proof is that at each iteration of the control algorithm the state vector of the multi-DOF brachiation robot's dynamics converges towards the temporary equilibrium and the temporary equilibrium in turn converges towards the reference trajectory. Thus, the control scheme exhibits global asymptotic stability properties and not local stability.[8] Assume the ith iteration of the control algorithm and the ith time interval about which a positive definite symmetric matrix P is obtained from the solution of the Riccati equation appearing in Eq. (61). By following the stages of the stability proof, one arrives at Eq. (70) which shows that the H-infinity tracking performance criterion holds. By selecting the attenuation coefficient ρ to be sufficiently small and in particular to satisfy $\rho^2 < ||e||_Q^2/||\tilde{d}||^2$ one has that the first derivative of the Lyapunov function is upper bounded by 0. Therefore, for the ith time interval it is proven that the Lyapunov function defined in Eq. (56) is a decreasing one. This signifies that between the beginning and the end of the ith time interval there will be a drop of the value of the Lyapunov function and since matrix P is a positive definite one, the only way for this to happen is the Euclidean norm of the state vector error e to be decreasing. This means that compared to the beginning of each time interval, the distance of the state vector error from 0 at the end of the time interval has diminished. Consequently, as the iterations of the control algorithm advance the tracking error will approach zero, and this is a global asymptotic stability condition. □

4.2. *State estimation with robust Kalman filtering*

The control loop has to be implemented with the use of information provided by a small number of sensors and by processing only a small number of state variables. To reconstruct the missing information about the state vector of the multi-DOF brachiation robot's dynamics it is proposed to use a filtering scheme and based on it to apply state estimation-based control.[8,39] The recursion of the H_∞ Kalman filter, for the model of the multi-DOF brachiation robot, can be formulated in terms of a *measurement update* and a *time update* part.

Measurement update:

$$\begin{aligned} D(k) &= [I - \theta W(k)P^-(k) + C^T(k)R(k)^{-1}C(k)P^-(k)]^{-1}, \\ K(k) &= P^-(k)D(k)C^T(k)R(k)^{-1}, \\ \hat{x}(k) &= \hat{x}^-(k) + K(k)[y(k) - C\hat{x}^-(k)]. \end{aligned} \tag{74}$$

Time update:

$$\begin{aligned} \hat{x}^-(k+1) &= A(k)x(k) + B(k)u(k), \\ P^-(k+1) &= A(k)P^-(k)D(k)A^T(k) + Q(k), \end{aligned} \tag{75}$$

where it is assumed that parameter θ is sufficiently small to assure that the covariance matrix $P^-(k)^{-1} - \theta W(k) + C^T(k)R(k)^{-1}C(k)$ will be positive definite. When $\theta = 0$ the H_∞ Kalman filter becomes equivalent to the standard Kalman filter. One can measure only a part of the state vector of the multi-DOF brachiation robot, such as state variables x_1, x_3, x_5, that is, the turn angles of the robot's joints, and can estimate through filtering the rest of the state vector elements. Moreover, the proposed Kalman filtering method can be used for sensor fusion purposes.

5. Simulation Tests

The performance of the proposed nonlinear optimal control scheme for the multi-DOF brachiation robot has been tested and confirmed through simulation

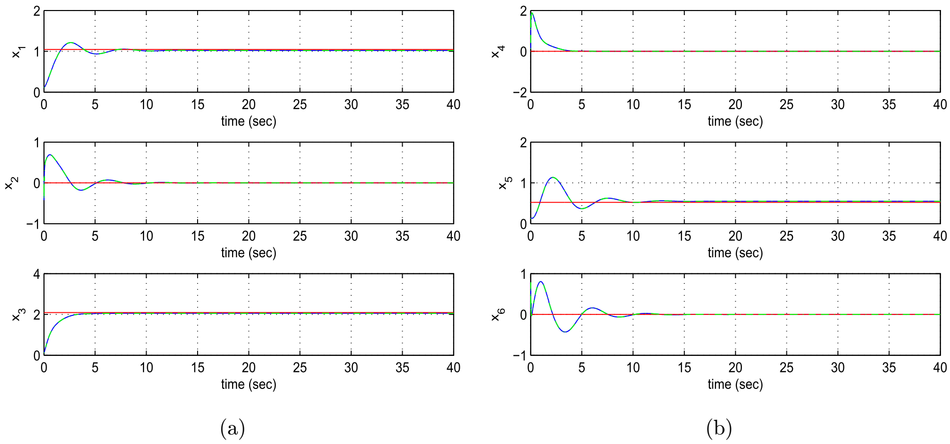

Fig. 3. Tracking of setpoint 1 by the multi-DOF brachiation robot. (a) Convergence of state variables x_1 to x_3, to the reference setpoints. (b) Convergence of state variables x_4 to x_6, to the reference setpoints.

experiments. The obtained results are depicted in Figs. 3–18. Indicative values for the simulation experiments have been $m_1 = 1\,\mathrm{kg}$, $l_1 = 1\,\mathrm{m}$, $m_2 = 1\,\mathrm{kg}$, $l_2 = 1\,\mathrm{m}$ and $m_3 = 0.5\,\mathrm{kg}$, $l_3 = 0.5\,\mathrm{m}$. It can be noticed that under the proposed nonlinear optimal control scheme, fast and accurate tracking of reference setpoints was achieved for all state variables of the underactuated brachiation robot. Besides, it can be noticed that the variations of the control inputs remained moderate, which signifies that the scheduled tasks can be accomplished by the brachiation robot under minimal energy consumption. This raises the autonomy and operational capacity of this robotic system. By limiting energy dispensing from the actuators of such robots one can

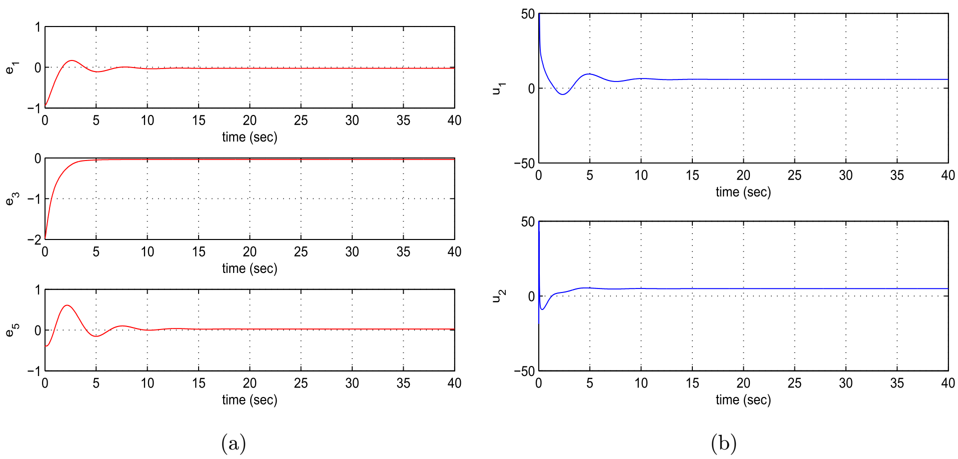

Fig. 4. Tracking of setpoint 1 by the multi-DOF brachiation robot. (a) Tracking error e_1, e_3 and e_5 of the joint angles of the brachiation robot. (b) Control inputs u_1 and u_2 generated by the actuators of the brachiation robot.

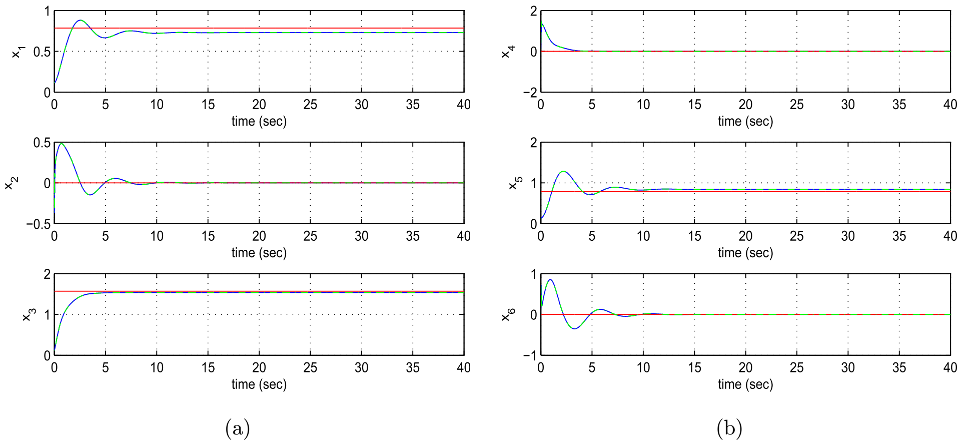

Fig. 5. Tracking of setpoint 2 by the multi-DOF brachiation robot. (a) Convergence of state variables x_1 to x_3, to the reference setpoints. (b) Convergence of state variables x_4 to x_6, to the reference setpoints.

ensure their uninterrupted functioning without the need for frequent recharging of batteries.

For the implementation of the nonlinear optimal control scheme in brachiation robots, the algebraic Riccati equation of Eq. (61) had to be repetitively solved at each time-step of the control algorithm. The values of parameters r, ρ and Q that appear in this Riccati equation determine also the transient performance of the control method. Actually, to achieve elimination of the tracking error for the state variables gain r has to be given a relatively small value, while to achieve fast convergence of the state variables to the reference setpoints, the elements of the diagonal matrix Q

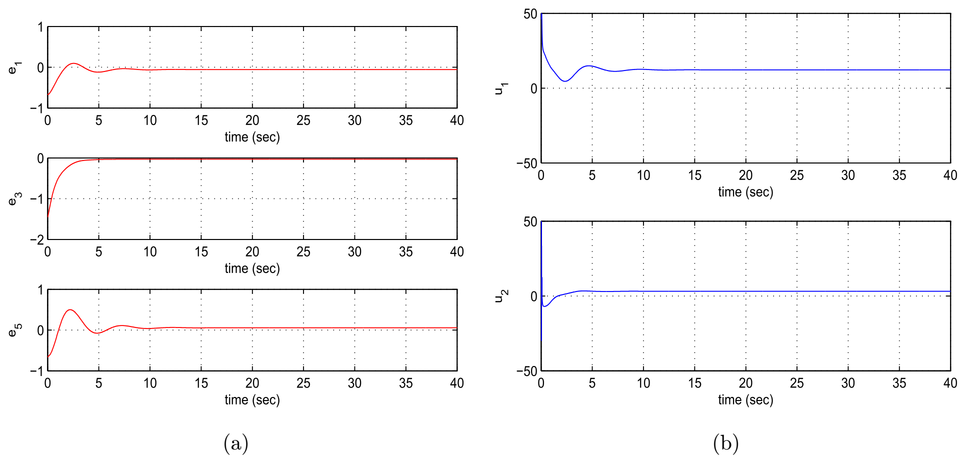

Fig. 6. Tracking of setpoint 2 by the multi-DOF brachiation robot. (a) Tracking error e_1, e_3 and e_5 of the joint angles of the brachiation robot. (b) Control inputs u_1 and u_2 generated by the actuators of the brachiation robot.

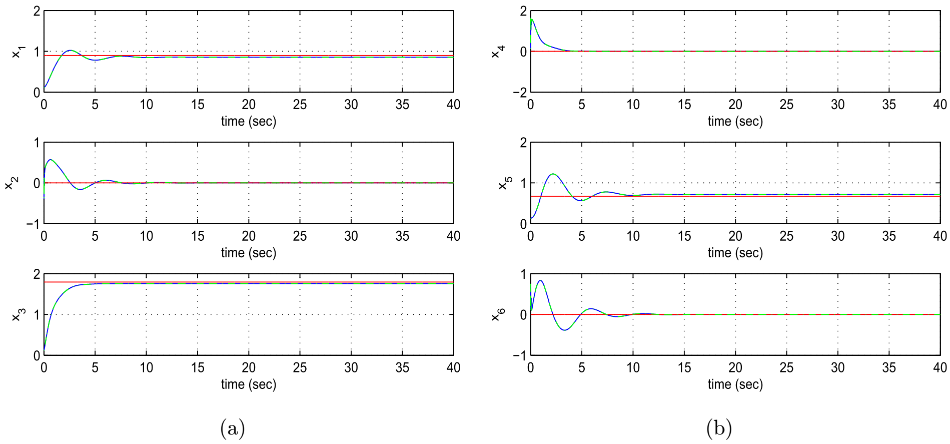

Fig. 7. Tracking of setpoint 3 by the multi-DOF brachiation robot. (a) Convergence of state variables x_1 to x_3, to the reference setpoints. (b) Convergence of state variables x_4 to x_6, to the reference setpoints.

have to be given relatively large positive values. Moreover, the attenuation coefficient ρ is the parameter that determines the robustness of the control scheme. The smallest value of ρ for which an acceptable solution can be obtained from the above-noted Riccati equation, in the form of a positive definite and symmetric matrix P, is the one that maximizes the disturbance rejection capability of the control scheme.

The aggregate simulation time was $T = 40\,\text{s}$. The adjustment time of each simulation experiment (time needed for the state variables of the robot to convergence to the targeted setpoints) did not exceed $10\,\text{s}$. The variation ranges of the control inputs in the individual simulation experiments (maximum and minimum values of the

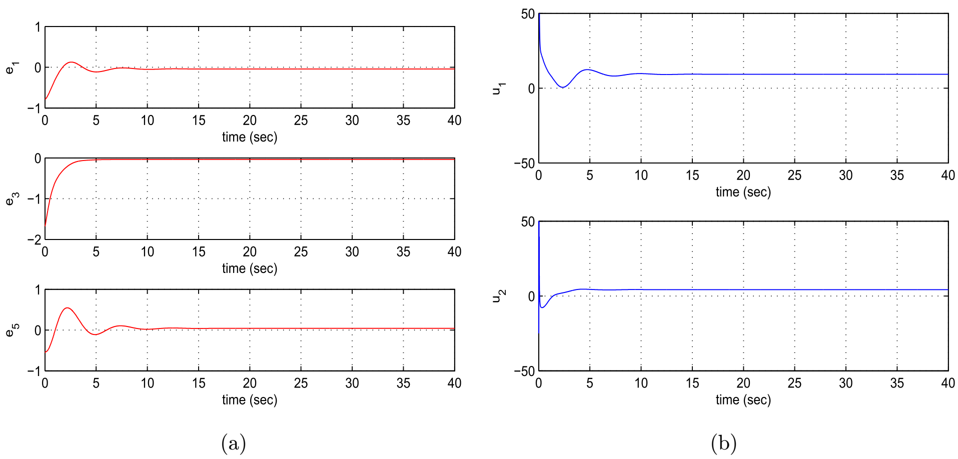

Fig. 8. Tracking of setpoint 3 by the multi-DOF brachiation robot. (a) Tracking error e_1, e_3 and e_5 of the joint angles of the brachiation robot. (b) Control inputs u_1 and u_2 generated by the actuators of the brachiation robot.

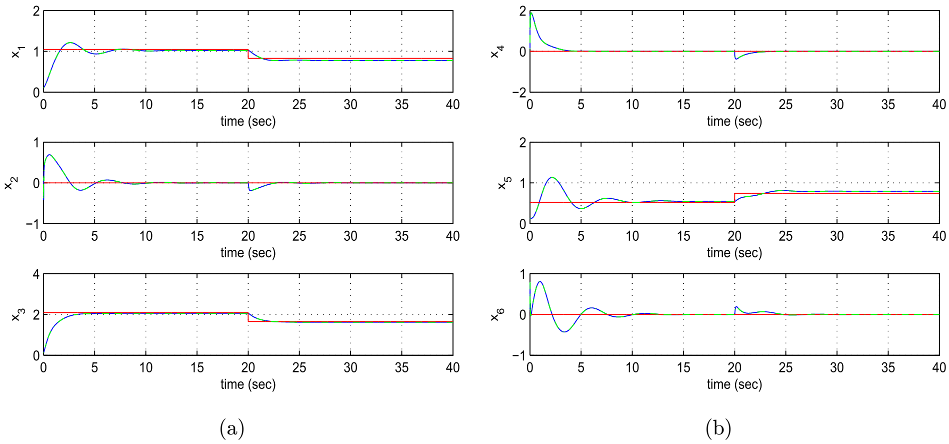

Fig. 9. Tracking of setpoint 4 by the multi-DOF brachiation robot. (a) Convergence of state variables x_1 to x_3, to the reference setpoints. (b) Convergence of state variables x_4 to x_6, to the reference setpoints.

torques generated by the actuators of the robot) were $[v_1^{\min}, v_1^{\max}] = [-200, 200]$, and $[v_2^{\min}, v_2^{\max}] = [-300, 300]$. Besides, the reference trajectories (setpoints) of the state variables of the brachiation robot were: (i) setpoint 1: $[\theta_1^d, \theta_2^d, \theta_3^d] = [\frac{\pi}{5}, \frac{2\pi}{5}, \frac{\pi}{2} - \frac{\pi}{5}]$, (ii) setpoint 2: $[\theta_1^d, \theta_2^d, \theta_3^d] = [\frac{\pi}{4}, \frac{2\pi}{4}, \frac{\pi}{2} - \frac{\pi}{4}]$, (iii) setpoint 3: $[\theta_1^d, \theta_2^d, \theta_3^d] = [\frac{\pi}{3.5}, \frac{2\pi}{3.5}, \frac{\pi}{2} - \frac{\pi}{3.5}]$, (iv) setpoint 4: $[\theta_1^d, \theta_2^d, \theta_3^d] = [\frac{\pi}{3}, \frac{2\pi}{3}, \frac{\pi}{2} - \frac{\pi}{3}]$ if $t \leq \frac{T}{2}$ and $[\theta_1^d, \theta_2^d, \theta_3^d] = [\frac{\pi}{3.8}, \frac{2\pi}{3.8}, \frac{\pi}{2} - \frac{\pi}{3.8}]$ if $t > \frac{T}{2}$, (v) setpoint 5: $[\theta_1^d, \theta_2^d, \theta_3^d] = [\frac{\pi}{2.6}, \frac{2\pi}{2.6}, \frac{\pi}{2} - \frac{\pi}{2.6}]$ if $t \leq \frac{T}{2}$ and $[\theta_1^d, \theta_2^d, \theta_3^d] = [\frac{\pi}{5}, \frac{2\pi}{5}, \frac{\pi}{2} - \frac{\pi}{5}]$ if $t > \frac{T}{2}$, (vi) setpoint 6: $[\theta_1^d, \theta_2^d, \theta_3^d] = [\frac{\pi}{4.2}, \frac{2\pi}{4.2}, \frac{\pi}{2} - \frac{\pi}{4.2}]$ if $t \leq \frac{T}{2}$ and $[\theta_1^d, \theta_2^d, \theta_3^d] = [\frac{\pi}{2.8}, \frac{2\pi}{2.8}, \frac{\pi}{2} - \frac{\pi}{2.8}]$ if $t > \frac{T}{2}$, (vii) setpoint 7: $[\theta_1^d, \theta_2^d, \theta_3^d] = [\frac{\pi}{4}, \frac{2\pi}{4}, \frac{\pi}{2} - \frac{\pi}{4}]$ if $t \leq \frac{T}{2}$

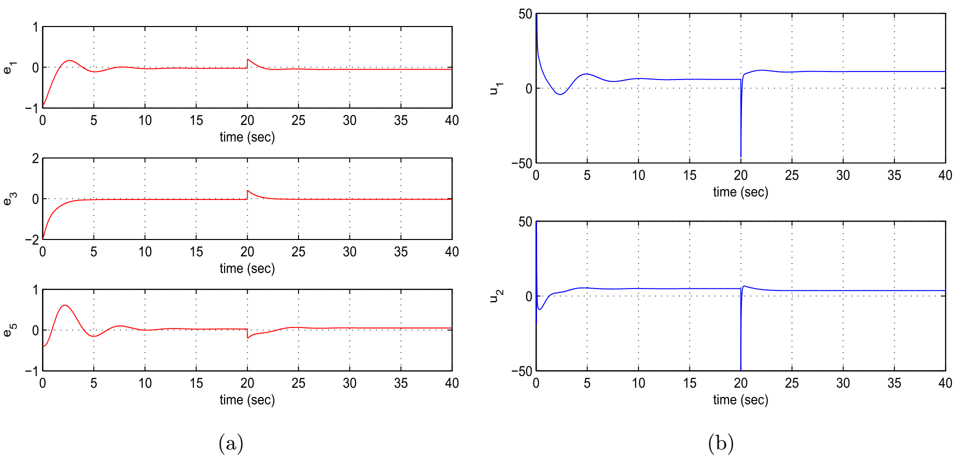

Fig. 10. Tracking of setpoint 4 by the multi-DOF brachiation robot. (a) Tracking error e_1, e_3 and e_5 of the joint angles of the brachiation robot. (b) Control inputs u_1 and u_2 generated by the actuators of the brachiation robot.

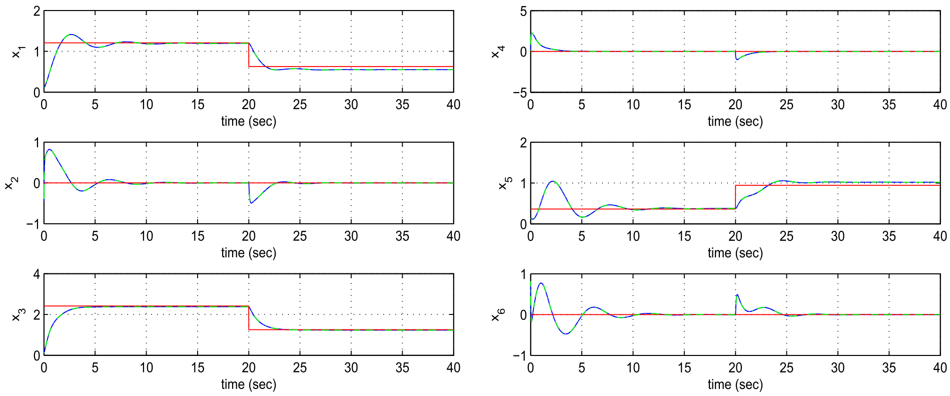

(a) (b)

Fig. 11. Tracking of setpoint 5 by the multi-DOF brachiation robot. (a) Convergence of state variables x_1 to x_3, to the reference setpoints. (b) Convergence of state variables x_4 to x_6, to the reference setpoints.

and $[\theta_1^d, \theta_2^d, \theta_3^d] = [\frac{\pi}{3}, \frac{2\pi}{3}, \frac{\pi}{2} - \frac{\pi}{3}]$ if $t > \frac{T}{2}$, (viii) setpoint 8: $[\theta_1^d, \theta_2^d, \theta_3^d] = [\frac{\pi}{3}, \frac{2\pi}{3}, \frac{\pi}{2} - \frac{\pi}{3}]$ if $t \leq \frac{T}{2}$ and $[\theta_1^d, \theta_2^d, \theta_3^d] = [\frac{\pi}{5}, \frac{2\pi}{5}, \frac{\pi}{2} - \frac{\pi}{5}]$ if $t > \frac{T}{2}$.

Comparing to other approaches for linear and nonlinear control of brachiation robots, the advantages of the proposed nonlinear optimal control method are justified as follows: (i) the method is conceptually simple because it avoids the complicated state variables transformations of global linearization-based control methods. The method is straightforward to apply since it only requires the existence of a solution from the algebraic Riccati equation that was noted before. The method does not come against singularity problems, (ii) the method is of proven global stability

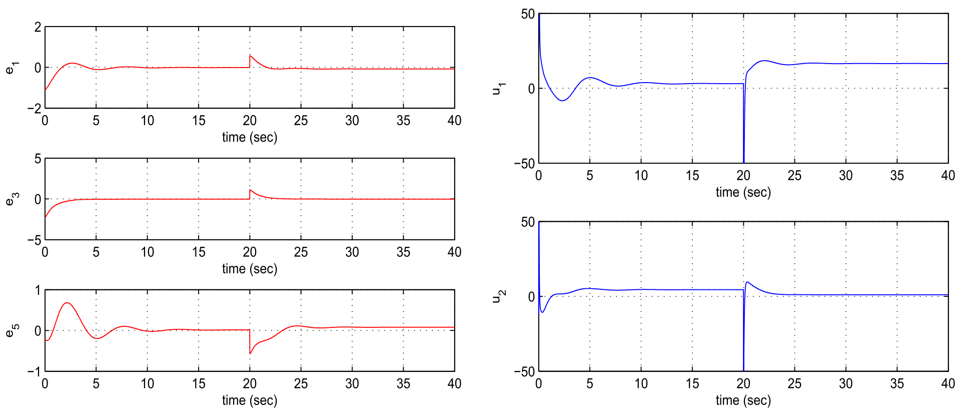

(a) (b)

Fig. 12. Tracking of setpoint 5 by the multi-DOF brachiation robot. (a) Tracking error e_1, e_3 and e_5 of the joint angles of the brachiation robot. (b) Control inputs u_1 and u_2 generated by the actuators of the brachiation robot.

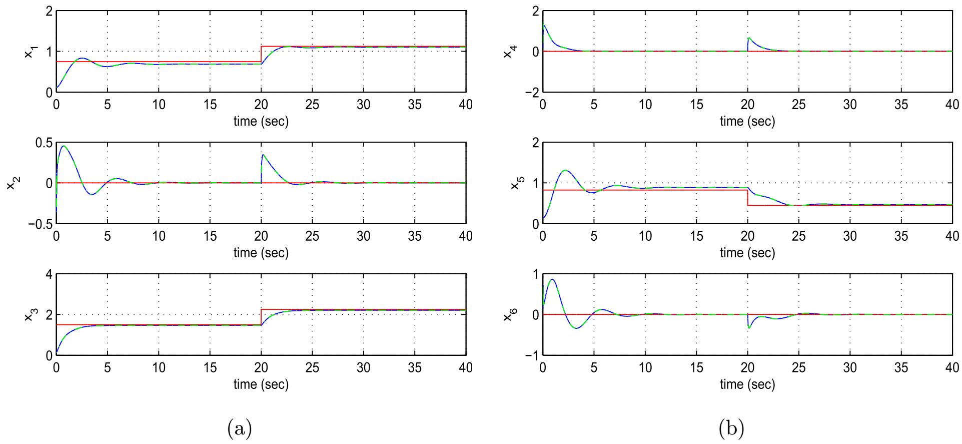

Fig. 13. Tracking of setpoint 6 by the multi-DOF brachiation robot. (a) Convergence of state variables x_1 to x_3, to the reference setpoints. (b) Convergence of state variables x_4 to x_6, to the reference setpoints.

and functions well under changes of operating points. The application of the method is not constrained to systems with a specific state-space form, (iii) the method is energy efficient because it keeps moderate the variation of the control inputs, thus also minimizing the consumption of energy by the actutators of the brachiation robot. The method is also computationally efficient because the above-noted Riccati equation can be solved in a time interval, that is, significantly smaller than the sampling period of the control scheme.

To elaborate on the tracking performance and on the robustness of the proposed nonlinear optimal control method for the three-link brachiation robot, the following

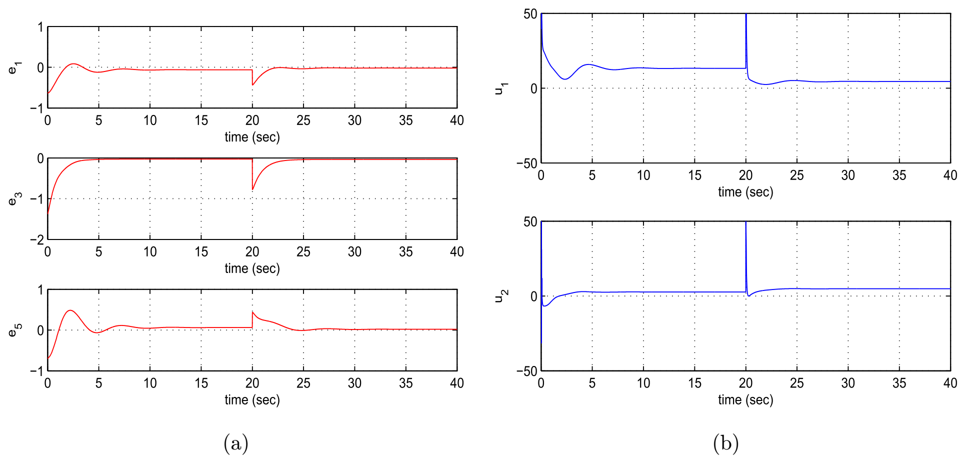

Fig. 14. Tracking of setpoint 6 by the multi-DOF brachiation robot. (a) Tracking error e_1, e_3 and e_5 of the joint angles of the brachiation robot. (b) Control inputs u_1 and u_2 generated by the actuators of the brachiation robot.

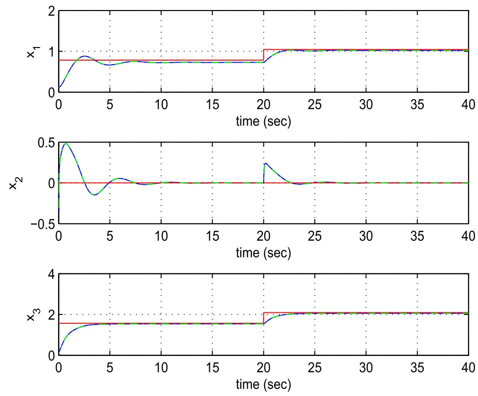

(a) (b)

Fig. 15. Tracking of setpoint 7 by the multi-DOF brachiation robot. (a) Convergence of state variables x_1 to x_3, to the reference setpoints. (b) Convergence of state variables x_4 to x_6, to the reference setpoints.

tables are given: (i) Table 1 which provides information about the accuracy of tracking of the reference setpoints by the state variables of the brachiation robot under an exact model, (ii) Table 2 which provides information about the robustness of the control method to parametric changes in the model of the brachiation robot (change in parameters I_1, I_2 and I_3, that is, to the moments of inertia of the three links of the robot up to 60%), (iii) Table 3 which provides information about the precision in state variables' estimation, that is, achieved by the H-infinity Kalman filter.

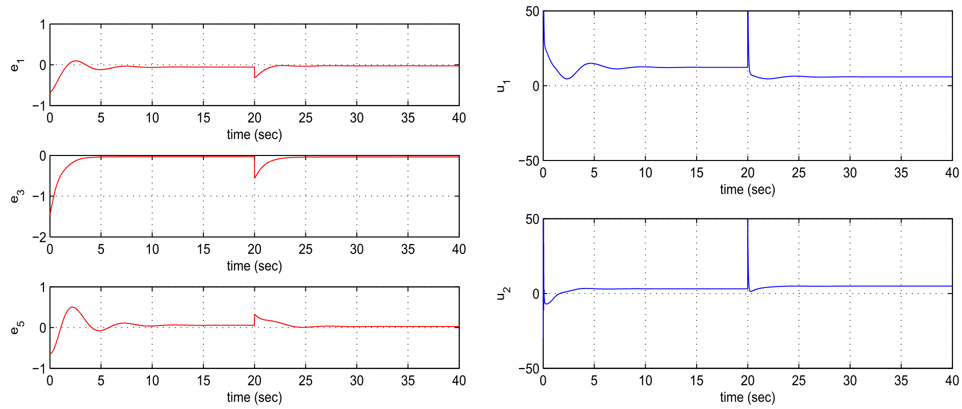

(a) (b)

Fig. 16. Tracking of setpoint 7 by the multi-DOF brachiation robot. (a) Tracking error e_1, e_3 and e_5 of the joint angles of the brachiation robot. (b) Control inputs u_1 and u_2 generated by the actuators of the brachiation robot.

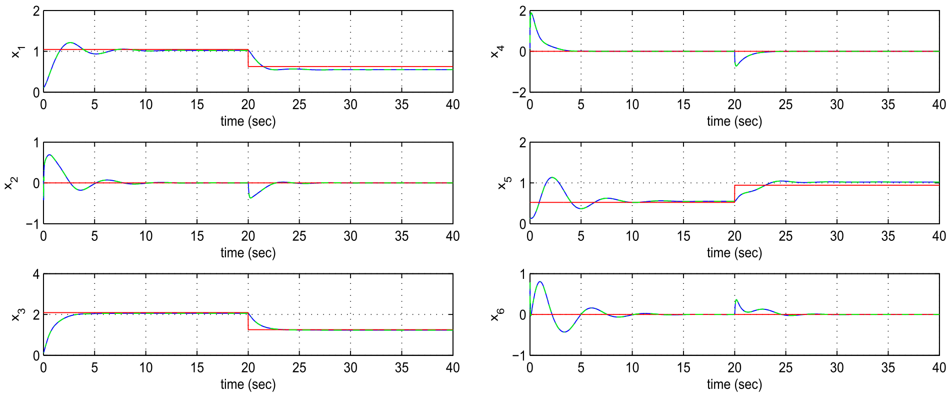

(a) (b)

Fig. 17. Tracking of setpoint 8 by the multi-DOF brachiation robot. (a) Convergence of state variables x_1 to x_3, to the reference setpoints. (b) Convergence of state variables x_4 to x_6, to the reference setpoints.

Finally, this paper's scientific contribution is outlined as follows: (i) the presented nonlinear optimal control method has improved performance when compared against other nonlinear control schemes that one can consider for the dynamic model of brachiation robots (such as Lie algebra-based control, differential flatness theory-based control, model-based predictive control, nonlinear model-based predictive control, sliding-mode control, backstepping control, etc.), (ii) it achieves fast and accurate tracking of all reference setpoints for the brachiation robot under moderate variations of the control inputs, (iii) it minimizes the consumption of energy by the

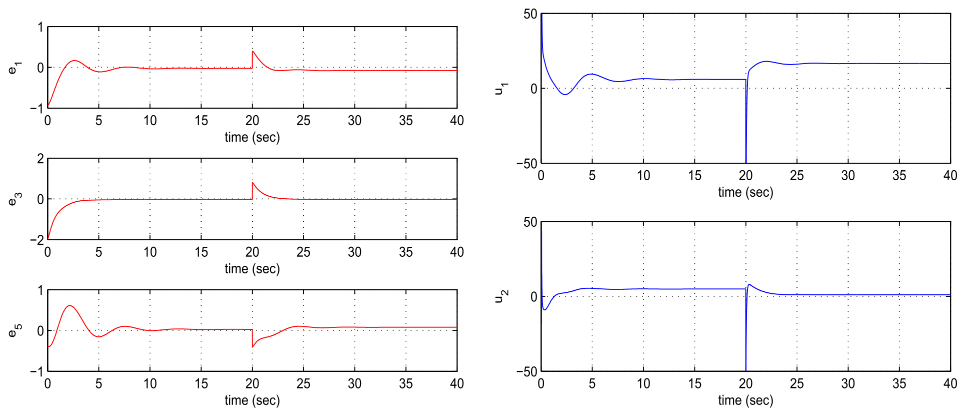

(a) (b)

Fig. 18. Tracking of setpoint 8 by the multi-DOF brachiation robot. (a) Tracking error e_1, e_3 and e_5 of the joint angles of the brachiation robot. (b) Control inputs u_1 and u_2 generated by the actuators of the brachiation robot.

November 7, 2021 9:04:35am WSPC/191-IJHR 2150015 ISSN: 0219-8436

Table 1. RMSE for the brachiation robot without disturbances.

	RMSE_{x_1}	RMSE_{x_2}	RMSE_{x_3}	RMSE_{x_4}	RMSE_{x_5}	RMSE_{x_6}
setpoint_1	0.0015	0.0001	0.0030	0.0001	0.0016	0.0003
setpoint_2	0.0047	0.0001	0.0029	0.0001	0.0048	0.0002
setpoint_3	0.0033	0.0001	0.0034	0.0001	0.0035	0.0002
setpoint_4	0.0034	0.0036	0.0051	0.0061	0.0033	0.0033
setpoint_5	0.0086	0.0096	0.0153	0.0163	0.0098	0.0083
setpoint_6	0.0074	0.0067	0.0096	0.0076	0.0098	0.0055
setpoint_7	0.0058	0.0047	0.0098	0.0072	0.0077	0.0038
setpoint_8	0.0070	0.0074	0.0088	0.0096	0.0066	0.0063

Table 2. RMSE for the brachiation robot under disturbances.

$\Delta a\%$	RMSE_{x_1}	RMSE_{x_2}	RMSE_{x_3}	RMSE_{x_4}	RMSE_{x_5}	RMSE_{x_6}
0%	0.0039	0.0001	0.0034	0.0001	0.0035	0.0001
10%	0.0033	0.0001	0.0034	0.0001	0.0035	0.0003
20%	0.0033	0.0001	0.0035	0.0001	0.0033	0.0003
30%	0.0033	0.0002	0.0035	0.0001	0.0033	0.0004
40%	0.0032	0.0002	0.0035	0.0001	0.0028	0.0005
50%	0.0032	0.0003	0.0036	0.0001	0.0027	0.0007
60%	0.0031	0.0003	0.0036	0.0001	0.0026	0.0008

Table 3. RMSE for the estimation performed by the *H*-infinity Kalman Filter (KF).

	RMSE_{x1}	RMSE_{x2}	RMSE_{x3}	RMSE_{x4}	RMSE_{x5}	RMSE_{x6}
setpoint_1	$0.3192 \cdot 10^{-6}$	$0.3062 \cdot 10^{-6}$	$0.6394 \cdot 10^{-6}$	$0.9318 \cdot 10^{-6}$	$0.3903 \cdot 10^{-6}$	$0.0898 \cdot 10^{-6}$
setpoint_2	$0.0364 \cdot 10^{-4}$	$0.0466 \cdot 10^{-4}$	$0.1071 \cdot 10^{-4}$	$0.1401 \cdot 10^{-4}$	$0.0130 \cdot 10^{-4}$	$0.0156 \cdot 10^{-4}$
setpoint_3	$0.1890 \cdot 10^{-5}$	$0.2134 \cdot 10^{-5}$	$0.4760 \cdot 10^{-5}$	$0.6454 \cdot 10^{-5}$	$0.0282 \cdot 10^{-5}$	$0.0680 \cdot 10^{-5}$
setpoint_4	$0.2852 \cdot 10^{-6}$	$0.0518 \cdot 10^{-6}$	$0.2492 \cdot 10^{-6}$	$0.1598 \cdot 10^{-6}$	$0.2781 \cdot 10^{-6}$	$0.0170 \cdot 10^{-6}$
setpoint_5	$0.2245 \cdot 10^{-5}$	$0.2544 \cdot 10^{-5}$	$0.6185 \cdot 10^{-5}$	$0.8010 \cdot 10^{-5}$	$0.0691 \cdot 10^{-5}$	$0.0870 \cdot 10^{-5}$
setpoint_6	$0.1008 \cdot 10^{-4}$	$0.1330 \cdot 10^{-4}$	$0.2942 \cdot 10^{-4}$	$0.3914 \cdot 10^{-4}$	$0.0349 \cdot 10^{-4}$	$0.0464 \cdot 10^{-4}$
setpoint_7	$0.1636 \cdot 10^{-5}$	$0.2195 \cdot 10^{-5}$	$0.4997 \cdot 10^{-5}$	$0.6438 \cdot 10^{-5}$	$0.0734 \cdot 10^{-5}$	$0.0687 \cdot 10^{-5}$
setpoint_8	$0.0248 \cdot 10^{-4}$	$0.0355 \cdot 10^{-4}$	$0.0756 \cdot 10^{-4}$	$0.1069 \cdot 10^{-4}$	$0.0109 \cdot 10^{-4}$	$0.0128 \cdot 10^{-4}$

actuators of the brachiation robot, thus achieving the cost-efficient functioning of this robotic system.

6. Conclusions

Control of brachiation robots is an important problem since such robots can be used in several inspection and maintenance tasks for critical infrastructure (as for instance the cable lines of the electricity grid). This control problem is nontrivial because of the nonlinear dynamics and the multivariable structure of these robots, as well as because of underactuation. In this paper, a novel nonlinear optimal (*H*-infinity) control method is proposed for multi-DOF brachiation robots. First, the dynamic model of these robots undergoes approximate linearization around a temporary operating point which is recomputed at each iteration of the control algorithm. The linearization procedure is based on first-order Taylor series expansion and on the computation of the related computation matrices. For the approximately linearized model of the robotic system, a stabilizing *H*-infinity feedback controller has been designed.

The proposed *H*-infinity controller achieves solution of the optimal control problem for the nonlinear dynamics of the brachiation robots under model uncertainty and external perturbations. Actually, this controller represents a min–max differential game taking place between (i) the control inputs which try to minimize a cost function that comprises a quadratic term of the state vector's tracking error (ii) the model uncertainty and exogenous disturbances which try to maximize this cost function. To compute the feedback gains of the *H*-infinity controller an algebraic Riccati equation had to be solved at each iteration of the control method. The global stability properties of the control scheme have been proven through Lyapunov stability analysis. The control method achieves fast and accurate tracking of setpoints by the state variables of the brachiation robot while keeping also moderate the variation of the control inputs. The latter property signifies that minimum energy is consumed by the actuators of the brachiation robot and that its autonomy and operational capacity are improved.

Appendix A. Euler–Lagrange Analysis for Modeling of the Brachiation Robot's Dynamics

In the inertial reference frame, the coordinates of the centers of gravity of the three links are

$$\begin{aligned}
x_{c_1} &= \frac{l_1}{2}\cos(\theta_1), & y_{c_1} &= (l_1+l_2) - \frac{l_1}{2}\sin(\theta_1),\\
x_{c_2} &= \frac{l_1}{2}\cos(\theta_1) + \frac{l_2}{2}\cos(\theta_1+\theta_2), & y_{c_2} &= (l_1+l_2) - \frac{l_1}{2}\sin(\theta_1) - \frac{l_2}{2}\sin(\theta_1+\theta_2),\\
x_{c_3} &= \frac{l_1}{2}\cos(\theta_1) + \frac{l_3}{2}\cos(\theta_1+\theta_3), & y_{c_3} &= (l_1+l_2) - \frac{l_1}{2}\sin(\theta_1) - \frac{l_3}{2}\sin(\theta_1+\theta_3).
\end{aligned} \tag{A.1}$$

The kinetic energy of the first link of the robot is

$$\begin{aligned}
K_1 &= \frac{1}{2}m_1(\dot{x}_{c_1}^2 + \dot{y}_{c_1}^2) + \frac{1}{2}I_1\dot{\theta}_1^2 \Rightarrow\\
K_1 &= \frac{1}{2}m_1\left[-\left(\frac{l_1}{2}\sin(\theta_1)\dot{\theta}_1\right)^2\right] + \left(\frac{l_1}{2}\cos(\theta_1)\dot{\theta}_1\right)^2 + \frac{1}{2}I_1\dot{\theta}_1^2 \Rightarrow\\
K_1 &= \frac{1}{2}m_1\frac{l_1^2}{4}\dot{\theta}_1^2 + \frac{1}{2}I_1\dot{\theta}_1^2.
\end{aligned} \tag{A.2}$$

The potential energy of the first link of the robot is

$$P_1 = m_1 g\left(l_1 + l_2 - \frac{l_1}{2}\sin(\theta_1)\right). \tag{A.3}$$

The kinetic energy of the second link of the robot is

$$\begin{aligned}
K_2 &= \frac{1}{2}m_2(\dot{x}_{c_2}^2 + \dot{y}_{c_2}^2) + \frac{1}{2}I_2(\dot{\theta}_1 + \dot{\theta}_2)^2 \Rightarrow \\
K_2 &= \frac{1}{2}m_2\Bigg[(-l_1\sin(\theta_1)\dot{\theta}_1 - \frac{l_2}{2}\sin(\theta_1+\theta_2)(\dot{\theta}_1+\dot{\theta}_2))^2 \\
&\quad + (-l_1\cos(\theta_1)\dot{\theta}_1 - \frac{l_2}{2}\cos(\theta_1+\theta_2)(\dot{\theta}_1+\dot{\theta}_2))^2\Bigg] + \frac{1}{2}I_2(\dot{\theta}_1+\dot{\theta}_2) \Rightarrow \\
K_2 &= \frac{1}{2}m_2\left[l_1^2\dot{\theta}_1^2 + \frac{l_2^2}{4}(\dot{\theta}_1+\dot{\theta}_2{}^2) + l_1 l_2\cos(\theta_2)\dot{\theta}_1(\dot{\theta}_1+\dot{\theta}_2)\right] + \frac{1}{2}I_2(\dot{\theta}_1+\dot{\theta}_2).
\end{aligned} \tag{A.4}$$

The potential energy of the second link of the robot is

$$P_2 = m_2 g\left(l_1 + l_2 - \frac{l_1}{2}\sin(\theta_1) - \frac{l_2}{2}\sin(\theta_1+\theta_2)\right). \tag{A.5}$$

The kinetic energy of the third link of the robot is

$$\begin{aligned}
K_3 &= \frac{1}{2}m_3(\dot{x}_{c_3}^2 + \dot{y}_{c_3}^2) + \frac{1}{2}I_2(\dot{\theta}_1 + \dot{\theta}_3)^2 \Rightarrow \\
K_3 &= \frac{1}{2}m_3\Bigg[(-l_1\sin(\theta_1)\dot{\theta}_1 - \frac{l_2}{2}\sin(\theta_1+\theta_3)(\dot{\theta}_1+\dot{\theta}_3))^2 \\
&\quad + (-l_1\cos(\theta_1)\dot{\theta}_1 - \frac{l_2}{2}\cos(\theta_1+\theta_2)(\dot{\theta}_1+\dot{\theta}_2))^2\Bigg] + \frac{1}{2}I_3(\dot{\theta}_1+\dot{\theta}_3) \Rightarrow \\
K_3 &= \frac{1}{2}m_3\left[l_1^2\dot{\theta}_1^2 + \frac{l_3^2}{4}(\dot{\theta}_1+\dot{\theta}_3{}^2) + l_1 l_3\cos(\theta_3)\dot{\theta}_1(\dot{\theta}_1+\dot{\theta}_3)\right] + \frac{1}{2}I_2(\dot{\theta}_1+\dot{\theta}_2).
\end{aligned} \tag{A.6}$$

The potential energy of the third link of the robot is

$$P_3 = m_3 g\left(l_1 + l_2 - \frac{l_1}{2}\sin(\theta_1) - \frac{l_3}{2}\sin(\theta_1+\theta_3)\right). \tag{A.7}$$

The Lagrangian of the brachiation robot is

$$\begin{aligned}
&L = K_1 + K_2 + K_3 - P_1 - P_2 - P_3 \Rightarrow \\
&L = \frac{1}{2}m_1\frac{l_1^2}{4}\dot{\theta}_1^2 + \frac{1}{2}I_1\dot{\theta}_1^2 + \frac{1}{2}m_2\left[l_1^2\dot{\theta}_1^2 + \frac{l_2^2}{4}(\dot{\theta}_1+\dot{\theta}_2{}^2) + l_1 l_2\cos(\theta_2)\dot{\theta}_1(\dot{\theta}_1+\dot{\theta}_2)\right] \\
&\quad + \frac{1}{2}I_2(\dot{\theta}_1+\dot{\theta}_2) + \frac{1}{2}m_3\left[l_1^2\dot{\theta}_1^2 + \frac{l_3^2}{4}(\dot{\theta}_1+\dot{\theta}_3{}^2) + l_1 l_3\cos(\theta_3)\dot{\theta}_1(\dot{\theta}_1+\dot{\theta}_3)\right] \\
&\quad + \frac{1}{2}I_2(\dot{\theta}_1+\dot{\theta}_2) - m_1 g\left(l_1 + l_2 - \frac{l_1}{2}\sin(\theta_1)\right) - m_2 g\Bigg(l_1 + l_2 - \frac{l_1}{2}\sin(\theta_1) \\
&\quad - l_2 2\sin(\theta_1+\theta_2)\Bigg) - m_3 g\left(l_1 + l_2 - \frac{l_1}{2}\sin(\theta_1) - l_3 2\sin(\theta_1+\theta_3)\right).
\end{aligned} \tag{A.8}$$

It is considered that actuation is applied only to the first and second link while the third link of this robotic system is unactuated. Consequently, the brachiation robot of Fig. 1 is underactuated. By applying the Euler–Lagrange method, one obtains the equations of the dynamics of the brachiation robot[8]

$$\frac{\partial}{\partial t}\frac{\partial L}{\partial \dot{\theta}_1} - \frac{\partial L}{\partial \theta_1} = T_1 - F_{v_1}, \tag{A.9}$$

$$\frac{\partial}{\partial t}\frac{\partial L}{\partial \dot{\theta}_2} - \frac{\partial L}{\partial \theta_2} = T_2 - F_{v_2}, \tag{A.10}$$

$$\frac{\partial}{\partial t}\frac{\partial L}{\partial \dot{\theta}_3} - \frac{\partial L}{\partial \theta_3} = -F_{v_3}. \tag{A.11}$$

From Eq. (A.9), and by considering that $F_{v_1} = b_1\dot{\theta}_1$, one obtains

$$\begin{aligned}
&\left[m_1\frac{l_1^2}{2} + I_1 + m_2 l_1^2 + m_2\frac{l_2^2}{4} + I_2 + m_3 l_1^2 + m_3\frac{l_3^2}{4} + m_2 l_1 l_2\cos(\theta_2) + I_3\right.\\
&\quad + m_3 l_1 l_3\cos(\theta_3)]\,\ddot{\theta}_1 + \left[m_2\frac{l_2^2}{4} + I_2 + m_2 l_1 l_2\cos(\theta_2)\right]\dot{\theta}_2 + \left[m_3\frac{l_3^2}{4} + I_3\right.\\
&\quad \left. + m_3 l_1 l_3\cos(\theta_3)\right]\ddot{\theta}_3 + \left[-m_2 l_1 l_2\sin(\theta_2)\dot{\theta}_2\left(\dot{\theta}_1 + \frac{\dot{\theta}_2}{2}\right) - m_3 l_1 l_3\sin(\theta_3)\dot{\theta}_3\right.\\
&\quad \left.\times\left(\dot{\theta}_1 + \frac{\dot{\theta}_3}{2}\right)\right] + \left[m_1 g\frac{l_2}{2}\cos(\theta_1) + m_2 g l_1\cos(\theta_2) + m_2 g\frac{l_2}{2}\cos(\theta_1+\theta_2)\right.\\
&\quad \left. + m_3 g l_1\cos(\theta_1) + [m_3]g\frac{l_2}{2}\cos(\theta_1+\theta_3)\right] + b_1\dot{\theta}_1 = T_1.
\end{aligned} \tag{A.12}$$

From Eq. (A.10), and by considering that $F_{v_2} = b_2\dot{\theta}_2$, one obtains

$$\begin{aligned}
&\left[m_2\frac{l_2^2}{4} + m_2 l_1 l_2\cos(\theta_2) + I_2\right]\ddot{\theta}_1 + [m_2\frac{l_2^2}{4} + I_2]\,\ddot{\theta}_2 - m_2 l_1 l_2\sin(\theta_1)\dot{\theta}_1\dot{\theta}_2\\
&\qquad - m_2 g\frac{l_2}{2}\cos(\theta_1+\theta_2) + b_2\dot{\theta}_2 = T_2.
\end{aligned} \tag{A.13}$$

From Eq. (A.11), and by considering that $F_{v_3} = b_3\dot{\theta}_3$, one obtains

$$\begin{aligned}
&\left[m_3\frac{l_3^2}{4} + m_3 l_1 l_3\cos(\theta_3) + I_3\right]\ddot{\theta}_1 + \left[m_3\frac{l_3^2}{4} + I_3\right]\ddot{\theta}_3 - m_3 l_1 l_3\sin(\theta_1)\dot{\theta}_1\dot{\theta}_3\\
&\qquad - m_3 g\frac{l_3}{2}\cos(\theta_1+\theta_3) + b_3\dot{\theta}_3 = 0.
\end{aligned} \tag{A.14}$$

The above three equations constitute the dynamic model of the three-link brachiation robot, which can be written next in matrix form.

References

1. W. Wu, M. Huang and X. Gu, Underactuated control of bionic ape robot based on the energy pumping method and big damping condition turn-back angle feedback, *Rob. Auton. Syst.* **100** (2015) 119–131.
2. Z. Lu, K. Sekiyama, T. Aoyama, Y. Hosegawa, T. Kobayashi and T. Fukuda, Energetically efficient ladder descent motion with internal stress and body motion optimized for a multi-locomotion robot, *IEEE Trans. Ind. Electron.* **62**(8) (2015) 4972–4984.
3. O. Menendez, F. A. Auat Cheein, M. Perez and S. Kouro, Robotics in power systems: Enabling a more reliable and safe grid, *IEEE Ind. Electron. Mag.***11**(2) (2017) 22–34.
4. A. Meghdari, S. H. Lavasani, M. Norouzi and M. S. R. Mousavi, Minimum control effort trajectory planning and tracking of the CEDRA brachiation robot, *Robotica* **31**(7) (2013) 1119–1129.
5. V. Menezes de Oliveira and W. F. Lages, MPC applied to motion control of an underactuated brachiation robot, in *IEEE ETFA 2006, IEEE 2006 Conf. Emerging Technologies and Factory Automation* (IEEE, Prague, Czech Republic, 2006), pp. 985–988.
6. V. Menezes de Oliveira and W. F. Lages, Control of a brachiating robot for inspection of aerial power lines, in *IEEE 2000 1st Int. Conf. Applied Robotics for the Power Industry* (IEEE, Montreal, Canada, 2010), pp. 1–6.
7. A. Meghdari, S. M. H. Lavasani, M. S. R. Mousavi and M. Norouzi, Optimal trajectory planning for brachiation robot on ladder with irregular branches, in *ASME 2011 International Design Engineering Technical Conf. and Computers and Information in Engineering Conf.* (ASME, Washington DC, USA, 2011), pp. 1131–1137.
8. G. Rigatos and K. Busawon, *Robotic Manipulators and Vehicles: Control, Estimation and Filtering* (Springer, Cham, 2018).
9. S. Farzen, A.-P. He, E. Davies and J. Rogers, Feedback motion planning and control of brachiating robots traversing flexible cables, in *IEEE ACC 2019, IEEE ACC 2019 American Control Conf.* (IEEE, Philadelphia, USA, 2019), pp. 1323–1329.
10. K.-D. Nguyen and D. Liu, Robust control of a brachiating robot, in *IEEE IROS 2017, IEEE 2017 Int. Conf. Intelligent Robots and Systems* (IEEE, Vancouver, Canada, 2017), pp. 6555–6560.
11. M. W. Gomes and A. L. Ruino, Five-link 2D brachiating ape model with life-like zero-energy-cost function, *J. Theor. Biol.* **257**(3) (2005) 265–278.
12. K. Ebrahimi and M. Navmar, Port-Hamiltonian control of a brachiating robot via generalized canonical transformations, in *IEEE ACC 2016, IEEE 2016 Automatic Control Conf.* (IEEE, Boston, Massachusetts, 2016), pp. 3026–3031.
13. J. Nakanishi, T. Fukuda and D. E. Koditschek, A brachiating robot controller, *IEEE Trans. Rob. Autom.* **16**(2) (2000) 109–124.
14. K.-D. Nguyen and D. Liu, Gibbon-inspired robust asymmetric brachiation along an upward slope, *Int. J. Control Autom. Syst.* **17**(10) (2019) 2647–2654.
15. E. H. Shata, P. Acharya and K.-D. Nguyen, Brachiating robot analysis and design, in *2019 IEEE Int. Conf. Electro Information Technology (EIT)* (IEEE, Brookings, USA, 2019), pp. 230–235.
16. V. Menezes de Oliveira and W. Fetter Lages, Control of a brachiation robot with a single underactuated joint using nonlinear model predictive control, in *IFAC SSSC 2007, IFAC 3rd Symp. Structure and Control* (IFAC, Foz de Iguessa, Brazil, 2007), pp. 430–435.
17. V. Menezes de Oliveria and W. Fetter Lages, Linear predictive control of a brachiation robot, in *IEEE 2006 Canadian Conf. Electrical and Computer Engineering* (IEEE, Ottawa, Canada, 2006), pp. 1518–1521.

18. V. Menezes de Oliveira and W. Fetter Lages, Predictive control of an underactuated brachiation robot, in *Proc. 8th IFAC Symposium on Robot Control* (IFAC, Bologna, Italy, 2006), pp. 19–24.
19. V. Menezes de Oliveira and W. Fetter Lages, Real-time predictive control of a brachiation robot, in *IEEE ETFA 2009, IEEE 2009 Conf. Emerging Technologies and Factory Automation* (IEEE, Mallorca, Spain, 2009), pp. 1–6.
20. Y. Yamukawa, Brachiation motion by a 2-DOF brachiating robot with hook-shaped end effectors, *Bull. JSME Mech. Eng. Lett.* **4** (2018) 1–9.
21. C.-Y. Lin and Z.-H. Yang, TRBR: Flight body posture compensation for transverse ricochetal brachiation robot, *Mechatronics* **65** (2020) 102307.
22. J. Nakanishi and S. Vijayakumar, Exploiting passive dynamics with variable stiffness actuation in robot brachiation, in *IEEE RSS 2012, IEEE 2012 Robotics Science and Systems Conf.* (IEEE, Sydney, Australia, 2012), pp. 305–310.
23. D. Liu and G. Yan, Motion control for an underactuated brachiation robot based on Lyapunov direct methods, *IOP Conf. Ser. Mater. Sci. Eng.* **768** (2020) 042040.
24. L. Yang, J. Fan, Y. Liu, E. Li, J. Pang and Z. Liang, A review on state-of-the-art power line inspection technologies, *IEEE Trans. Instrum. Meas.* **69**(12) (2020) 9350–9365.
25. K. Omoto, M. Dei and T. Ohtsuka, Integrated optimization of climbing locomotion for a humanoid robot, in *11th IFAC Symp. Nonlinear Control Systems, IFAC NOLCOS 2019* (IFAC, Vienna, Austria, 2019), pp. 574–579.
26. F. L. Moro, Balancing while executing computing reaching tasks: An attractor-based whole body motion control system using gravitational stiffness, *Int. J. Humanoid Rob.* **13**(1) (2016) 1550046.
27. M. Li, W. Guo, R. Lin, C. Wu and L. Moro, An efficient motion generation method for redundant humanoid robot arm based on the intrinsic principles of human arm motion, *Int. J. Humanoid Rob.* **15**(6) (2018) 1850026.
28. G. Yang, E. Li, C. Fan, W. Lei and Z. Liang, Modelling and control of a bi-brachiate inspection robot for power transmission lines, in *IEEE ICMA 2010, IEEE 2010 Int. Conf. Mechatronics and Automation* (IEEE, Xian, China, 2010), pp. 1036–1041.
29. G. Yang, E. Li, C. Fan, W. Lei and Z. Liang, Adaptive fuzzy logic-based inspection robot for high voltage power transmission lines, in *IEEE ICMA 2010, IEEE 2010 Int. Conf. Mechatronics and Automation* (IEEE, Xian, China, 2010), pp. 613–618.
30. G. Rigatos, P. Siano and C. Cecati, A new non-linear H-infinity feedback control approach for three-phase voltage source converters, *Electr. Power Compon. Syst.* **44**(3) (2015) 303–312.
31. G. Rigatos, P. Siano, P. Wira, K. Busawon and R. Binns, A nonlinear H-infinity control approach for autonomous truck and trailer systems, *Unmanned Syst.* **8** (2019) 49–69.
32. G. Rigatos, P. Siano, P. Wira and F. Profumo, Nonlinear H-infinity feedback control for asynchronous motors of electric trains, *Intell. Ind. Syst.* **1** (2015) 85–98.
33. G. Rigatos, K. Busawon, J. Pomares and M. Abbaszadeh, Nonlinear optimal control for the wheeled inverted pendulum, *Robotica* **38** (2019) 29–47.
34. G. Rigatos, P. Siano and M. Abbaszadeh, Nonlinear H-infinity control for 4-DOF underactuated overhead cranes, *Trans. Inst. Instrum. Control* **40** (2017) 2364–2377.
35. G. Rigatos and S. Tzafestas, Extended Kalman filtering for fuzzy modelling and multisensor fusion, *Math. Comput. Modell. Dyn. Syst.* **13** (2007) 251–266.
36. M. Basseville and I. Nikiforov, *Detection of Abrupt Changes: Theory and Applications* (Prentice-Hall, Hoboken, 1993).
37. G. Rigatos and Q. Zhang, Fuzzy model validation using the local statistical approach, *Fuzzy Sets Syst.* **60**(7) (2009) 882–904.

38. G. Rigatos, *Intelligent Renewable Energy Systems: Modelling and Control* (Springer, Cham, 2016).
39. G. Rigatos, *Nonlinear Control and Filtering Using Differential Flatness Approaches: Applications to Electromechanical Systems* (Springer, Cham, 2015).
40. G. J. Toussaint, T. Basar and F. Bullo, H_∞ optimal tracking control techniques for nonlinear underactuated systems, in *Proc. IEEE CDC 2000, 39th IEEE Conf. Decision and Control* (IEEE, Sydney Australia, 2000), pp. 2078–2083.